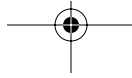
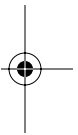


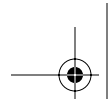
12 Nano/microstructure and Property Control of Single and Multiphase Materials

Philippe Colomban

CONTENTS

I. Introduction.....	304
II. Precursors and Analysis Methods.....	305
III. Densification.....	309
A. Gel Structure and Composition	309
B. Sintering	312
C. Multicomponent Materials.....	314
IV. Composites and Multiphase Materials	315
A. Particulate-Reinforced Materials	315
B. Metal- and Ceramic-Ceramic Nanocomposites	316
C. One-Dimensional and Two-Dimensional Fiber-Reinforced Composites.....	317
D. Three-Dimensional Fiber-Reinforced Composites: Near Net-Shape Sintering.....	318
E. Functionally Graded Materials	322
V. Characterization of Multiphase Materials	322
A. Depth-Sensing Microindentation.....	323
B. Micro-Raman Spectrometry	325
1. The Raman Effect in Nanomaterials.....	327
2. Correlation Between Raman Parameters and Grain Size	327
3. Raman Images	329
4. Prediction of Material Properties from Raman Parameters.....	330
5. Residual Stress/Strain in Multiphase Materials	332
VI. Summary	332
Acknowledgments	333
References	333

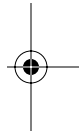




I. INTRODUCTION

One of the key steps in the advancement of ceramic processing is the achievement of a special, controlled and reproducible micro(nano)structure. Reducing the dimension of a “meso/macrosopic” phase down to the nanometer scale produces moieties in which interfacial volumes dominate. This results in absolutely unique properties. Sol-gel routes, and more generally synthesis through liquid precursors, offer the possibility to control the structure at the scale of the precursor and its aggregates (1 to 100 nm). This allows the preparation of more homogeneous materials than the usual ball-milling process. Materials made with (or from) nanophases have received considerable attention in the last few years, but their characterization is not easy. A large variety of nanomaterials are now being developed, if not already commercially available, for applications taking advantage of their (1) optical properties (pigments in traditional ceramics and for the cosmetics industry, fluorescent markers, quantum dots, photonic crystals for multiplexing and switching in optical networks, quantum computer components, etc.); (2) mechanical properties (fibers, wear-resistant, anticorrosion, and cutting coatings, “nanopolishing” SiC, diamond, boron carbide powders, high impact strength nanocomposites, etc.); (3) magnetic properties (data storage, reading heads, giant magnetoresistance [GMR] materials, etc.); (4) high specific surface area (propulsion, filters, nanosensors, semiconductor nanowires, catalysts, etc.); (5) electrical properties (miniaturized silicon chips, single electron transistors, carbon nanotubes or even silicon nanotubes transistors, etc.); and (6) biocompatibility (*in vivo* drug delivery, diagnostic and monitoring devices, etc.). Most of these materials are ceramics synthesized through a route involving a liquid step. In fact, potters and ceramists have been using such nanoscience (clays form a “physical” gel; Figure 12.1a) for thousands of years in clay-based ceramics: most of the properties of traditional ceramics (plasticity, shapability, rheology, low sintering temperature, etc.) are directly related to the fact that natural clay—the raw material—is nanosized and the so-called sol-gel route only results from the transposition of the clay route to simpler oxide, carbide, etc. compositions.^{1,2} In the last 10 centuries, nanosized ceramic pigment powders were also created to color enamels and glass.³ Because of human eye sharpness, pigment must have a particle size close to 100 nm to give homogeneous coloration.

The challenge for ceramists is to achieve perfect control on related properties. This obviously requires correlating the parameters of the synthesis process with the resulting nano/microstructure. This chapter focuses on the ways to prepare multiphase materials and their main controlling parameters, on the precursors and their structure, and on the porosity, densification, and final mechanical properties. The goal here is not to give a complete overview, but to address the most important points and the ways to solve most of the problems with some examples. Particular attention will be given to nondestructive methods able to characterize the materials over different scales (from atomic distances to full size).



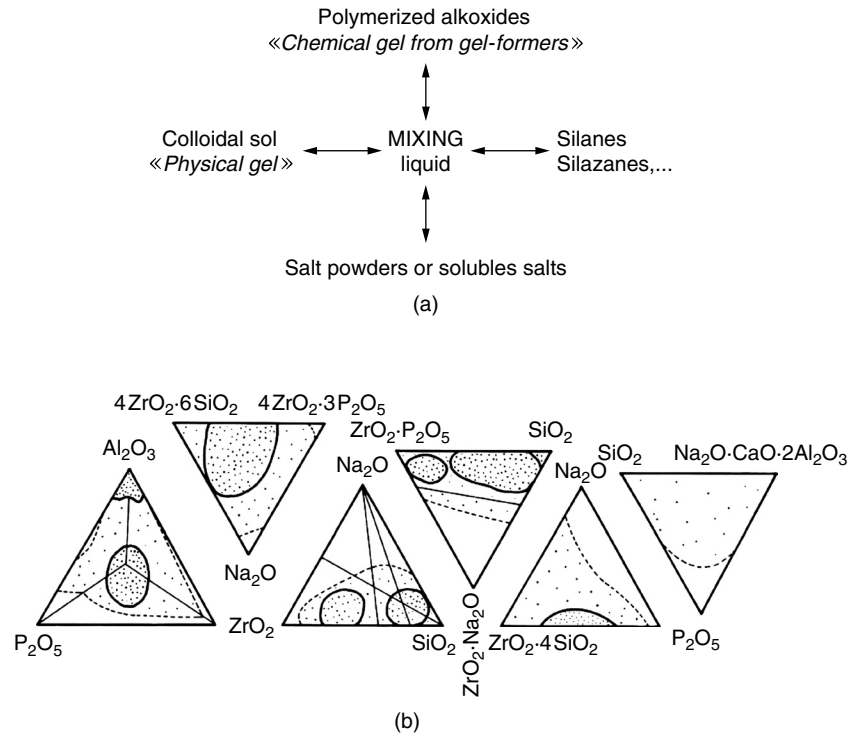
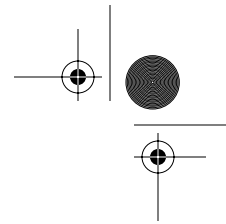


FIGURE 12.1 (a) Schematic flowchart of hybrid routes. (b) Sol-gel forming compositions (alkoxide route) in the $\text{SiO}_2\text{-Al}_2\text{O}_3\text{-ZrO}_2\text{-P}_2\text{O}_5$, $4\text{ZrO}_2\cdot 6\text{SiO}_2\text{-Na}_2\text{O-}4\text{ZrO}_2\cdot 3\text{P}_2\text{O}_5$, $\text{ZrO}_2\text{-Na}_2\text{O-SiO}_2$, $\text{ZrO}_2\cdot \text{P}_2\text{O}_5$, $\text{ZrO}_2\cdot \text{Na}_2\text{O-SiO}_2$, $\text{ZrO}_2\cdot 4\text{SiO}_2\text{-Na}_2\text{O-P}_2\text{O}_5$, and $\text{SiO}_2\text{-P}_2\text{O}_5\text{-Na}_2\text{O-CaO}\cdot 2\text{Al}_2\text{O}_3$ phase diagrams. The representation corresponds to the final oxide composition. Solid line indicates the limit of optically clear gel by slow hydrolysis. Dashed line indicates the limit of easy synthesis of (translucent) monolithic gels. (Reprinted from Colombari, P., Gel technology in ceramics, glass-ceramics and ceramic-ceramic composites, *Ceram. Int.*, 15, 23, 1989. With permission from Elsevier.)

II. PRECURSORS AND ANALYSIS METHODS

Precursors must have different properties:⁴⁻¹⁴ (1) a high content of the final elements (mostly aluminum, silicon, zirconium, titanium, phosphorus), (2) a low content of health hazardous elements and elements that corrode the equipment (e.g., chlorine, sulfur), (3) a viscosity adapted to the process: low viscosity for preform infiltration, medium viscosity for spinning and coating, (4) a controlled precursor-ceramic transformation (bubbling is researched for foams but not for dense parts), (5) the ability to be mixed with other precursors or to be processed ("good" hydrolysis rate), and (6) low cost.

Regarding sol-gel routes, the most used reagents are those made with gel-former compositions: aluminium-s-butoxide $[\text{Al}(\text{OC}_4\text{H}_9)_3]$, tetraethoxysilane $[\text{Si}(\text{OC}_2\text{H}_5)_4]$ (and homologous methoxysilane), aluminum-silicon ester

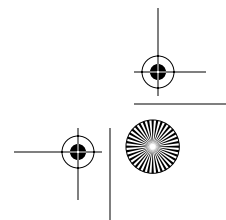
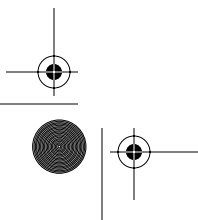


$[(OC_4H_9)_2-Al-O-Si(OC_2H_5)_3]$, zirconium-i-propoxide $[Zr(OC_3H_7)_4]$, titanium butoxide $[Ti(OC_4H_9)_4]$ and propoxide $[Ti(OC_3H_7)_4]$, tributylborate $[B-(OC_4H_9)_3]$, and tributylphosphate $[P-(OC_4H_9)_3]$.⁶⁻¹⁷ Figure 12.1b shows the basic $SiO_2-Al_2O_3-ZrO_2-P_2O_5$ quaternary diagram and some related ternary diagrams. The dotted regions correspond to composition ranges easily giving optically clear (high dot density) or translucent (low dot density) gels. The dashed line corresponds to the limit of easy synthesis. The handling of aluminum and some other reagents like germanium propoxide $[Ge(OC_3H_7)_4]$ requires a glove box free of H_2O traces. Homemade preparations of very hygroscopic alkoxides guarantees their quality. However, in the preparation of multicomponent materials through the sol-gel route or by mixing organic precursors, determination of the metal element content is not obvious.⁷ In commercially available reagents, the metal content often varies from batch to batch and a slight prehydrolysis is often observed. The degree of hydrolysis can be determined by nuclear magnetic resonance (NMR), infrared (IR) absorption, or Raman scattering.^{14,16-18} This modifies the metal content and the viscosity. The viscosity of the alkoxides can be adjusted at values of approximately 1 poise by heating below $80^\circ C$ for most of the reagents. Mixing of liquid precursors promotes the intimate combination of various precursors at the molecular scale and allows adjustment of the viscosity to void filling requirements.

One of the main interests of liquid alkoxides is that they exhibit a rather good ceramic yield: typically the alkoxide-to-ceramic conversion yield is between 20 and 30 wt%. Thermal treatments under various atmospheres (NH_3 , H_2S , CO) lead to (oxy)-nitrides, -sulfides, -carbides, and derivatives.^{1,19} However, carbides, nitrides, and their oxyderivatives are generally prepared by cross-linking and ceramization of specific precursors: polycarbosilanes, polysilazanes. Since the work of Yajima et al.,^{20,21} polycarbosilane (PCS) is well known as a precursor of SiC materials.^{22,23} The high viscosity of this precursor is convenient for fiber spinning, but prevents its use to fill a fiber preform already filled with a submicrometer powder. Unfortunately the oxygen-driven reticulation of the chains of the precursor, convenient for films and fiber, is not obvious inside a thick sample, which makes it difficult to control the stoichiometry in the whole. Polyvinylsilane (PVS) fulfills the specific requirements for the infiltration of a porous body:²² (1) a thermostat behavior with a cross-linking temperature ($200^\circ C$ to $300^\circ C$) far enough from the beginning of pyrolysis ($400^\circ C$) to avoid formation of bubbles during the cycle; (2) a relatively low molecular weight (MW < 1000), which ensures a sufficiently low viscosity (e.g., 0.3 poise at $130^\circ C$) to allow injection in the fiber preform at "low" temperatures; (3) a very high ceramic yield: 64% in weight; and (4) a silicon/carbon stoichiometry leading to air-stable materials. A variety of precursors of carbide, nitrides, and their mixture are now available for many applications. Last-generation precursors use γ radiation to develop an intrinsic cross-linking between precursor chains instead of the extrinsic Si-O-Si bridging obtained by controlled oxidation.

Generally, the main questions that need an answer are:

Is the expected composition and structure achieved? Most of the materials prepared through liquid precursor routes are first obtained in an



amorphous or metastable form. These forms are very similar to those obtained by quenching from a high-temperature melt, but usually retain hydrogen (protons, OH groups, and $-CH$ branches).²⁴⁻²⁶ In the liquid state the local structure is determined by geometry constraints. On the contrary, in the solid state the structure of materials equilibrated at a given temperature is dominated by long-range Coulombic interactions. Knowledge of the phase relationship diagram is mandatory and thermal expansion measurement (Figure 12.2a) is the simplest way to determine it.^{4,25-28} Differential thermal analysis (DTA) and phase characterization methods (x-ray diffraction [XRD], Raman scattering, IR absorption) are useful methods to confirm the phase relationship.

Is the sample free of hydrogen? Sol-gel-prepared ceramics easily retain a few wt% of protons up to 1000°C or more, and these protons drive the sintering and crystallization mechanisms.^{24,26} Rather similar amounts of hydrogen are retained in carbides/nitrides derived from polymeric precursors (e.g., in SiC fibers thermally treated at approximately 1200°C). This hydrogen can generate unwanted gas departure.

Is the density/porosity convenient for the final use? What is the optimum processing temperature? Is the material homogeneous? What are the differences between the skin and the bulk? Where are the second phases located?

Another question is how to select the method with the lower cost. The use of hybrid methods in which part of the elements is introduced from metal-organic precursors offers the best compromise (Figure 12.1a).

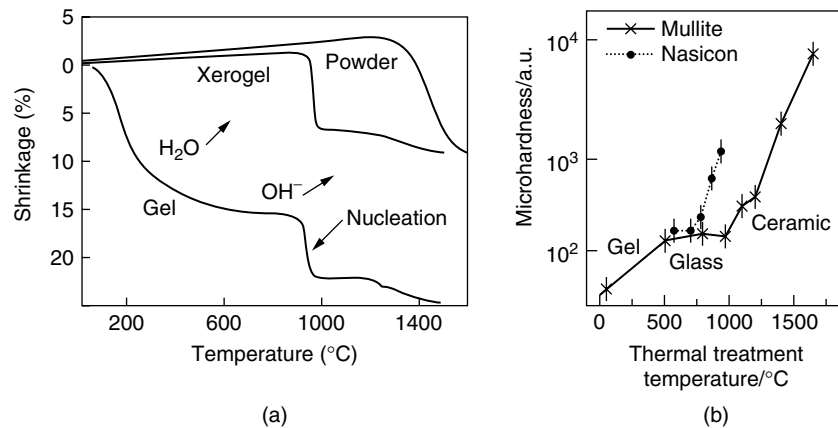
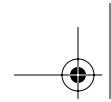


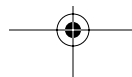
FIGURE 12.2 (a) Comparison of the linear shrinkage of mullite ($3Al_2O_3 \cdot 2SiO_2$) micronic powder, 600°C thermally treated gel (xerogel) and pristine gel. (After Reference 87.) (b) Plot of the R.T. microhardness for mullite and Nasicon ($Na_3Zr_2Si_3PO_{12}$) as a function of thermal treatment. (After Reference 27.)



The final question is how to control the achieved materials. Methods and representative references are listed in Table 12.1. Two of these methods, the depth-sensing indentation and the micro-Raman scattering, were developed recently and will be addressed in the last part of this chapter.

TABLE 12.1
Methods of Analysis for Nano/Microsized Materials

Sensitivity	Method	Information	Advantages	Drawbacks	Ref.
Bond length Structure	Dilatometry	Densification Phase transition Crystallization CTE Anharmonicity Sintering mechanisms	Analysis of the whole sample High sensitivity Easy atmosphere control	Generally destructive	4, 25–28
Bond length Structure Composition	DTA	Phase transformation /transition	Routine High sensitivity		4, 28
Bond length Structure Symmetry Composition Geometry	Vibrational spectroscopy (IR, Raman) Microspectros copies	Structure Crystallization Phase transition Strain/stress Phase location	Minor phases can be studied Phase and properties mapping Properties predictions	Very different cross sections	16, 51, 52, 89, 94, 107
Bond length Structure Symmetry	X-ray, electron (neutron) Diffraction (TEM)	Structure Phases	Good database	Destructive Materials to be crystalline	15
Composition Geometry	SEM	Phase locations			5
Density	Thermal expansion/ shrinkage	Sintering	Routine technique	Destructive	7, 36, 40
Density	Gas adsorption	Porosity Reactivity	Pore size and distribution	Very long time of analysis Difficulty of drying	30, 31
Density	X-ray (neutron) scattering	Phase contrast	Whole sample	Unequivocal	33, 38
Mass Composition	TG	Gas evolution Oxidation	Routine	Destructive	27, 31

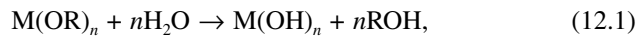


III. DENSIFICATION

We will take examples among silicates, aluminates, and zirconates prepared from the alkoxide sol-gel route that serve as the basic compounds for many applications. Figure 12.3 illustrates the structure change at the bond length scale when a gel/porous glass densifies by dehydroxylation-crystallization. The departure of some OH groups destabilizes the pore surface and gives rise to a high surface mobility. Rearrangement in the crystalline form induces densification.^{24,26} Consequently the microhardness increases (Figure 12.2b).²⁷ This sketch illustrates that the densification and crystallization process is intimately related to the gel structure.

A. GEL STRUCTURE AND COMPOSITION

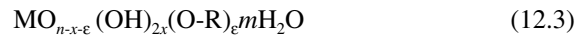
Gelation of liquid oxide precursors like alkoxides ($M(OR)_n$) results from hydrolysis-polycondensation:



and simultaneously, generally^{1,2,8-11,29}



After drying the resultant gel has a complex composition such as



with $x \sim 0.1$ to 0.3 , $m = 3$ to 6 , and $\epsilon \sim 0.01$.³⁰⁻³³ These gels are made of small polymeric entities (diameter 0.5 nm to 5 nm), which are more or less aggregated and densely packed according to the process (hydrolysis-polycondensation rate, initial alkoxide-to-solvent and alkoxide-to-water ratios).^{17,18,33} Small angle x-ray/neutron diffraction analysis and scanning electron microscopy (SEM)/transmission electron microscopy (TEM) images show that oxide gels are made of

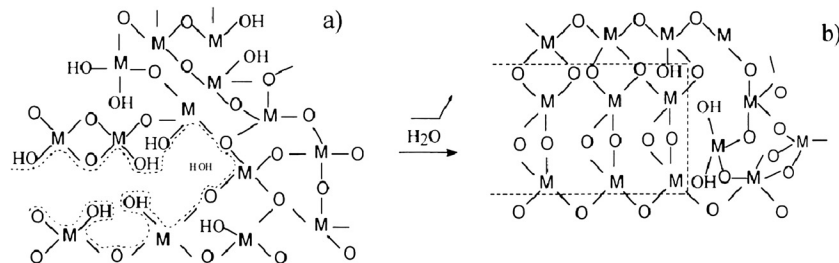


FIGURE 12.3 Sketch of the nucleation-densification process (b) involved with the dehydroxylation of a gel surface (a). (After Reference 27.)

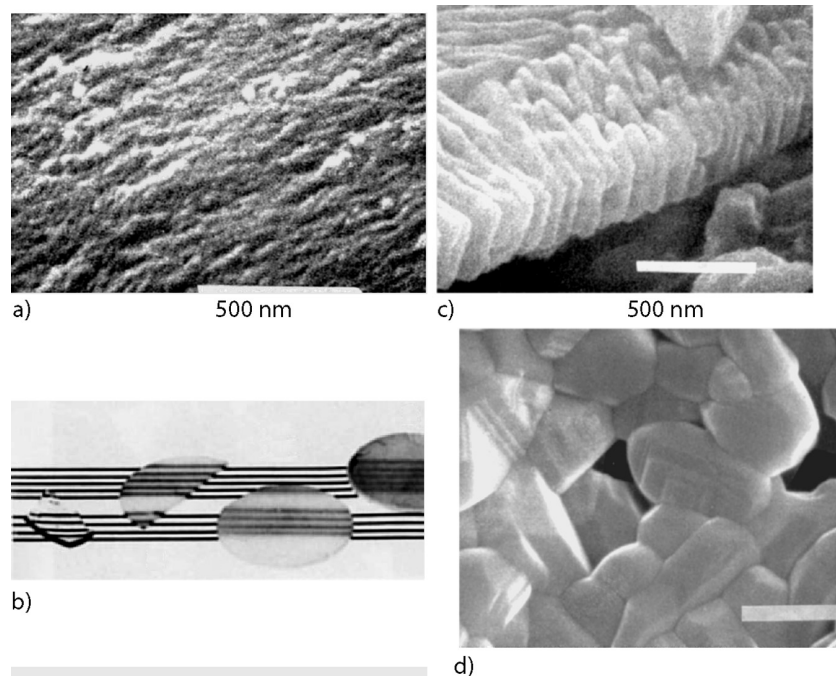
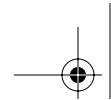


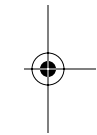
FIGURE 12.4 Scanning electron micrography of optically/translucent NASICON gels (a-c) prepared by different gels routes. An example of fine grained optically clear ceramic (1400°C fired mullite) is shown in (d) (a-d, reprinted from *Ceramic Powder Science and Technology*, Messing, G., Ed., © 1989, with permission from The American Ceramic Society; (d) after “Sciences & Techniques”, *Céramiques: les progrès de la Chimie*, © Ph. Colomban).

rather globular polymeric entities (diameter 1 nm to 2 nm), which are more or less densely packed according to the hydrolysis-polycondensation rate and the initial alkoxide-solvent-water ratios. An example is given in Figure 12.4: the size of the aggregated moieties is <20 nm. Dense packing of these aggregates is obtained by sedimentation (slow hydrolysis using an inert solvent) or by pressure (compaction of a gel powder prepared by rapid hydrolysis). Krypton, CO, argon, or N₂ Brunauer-Emmit-Teller (BET) measures the equivalent diameters of the pores. By definition, pores with diameters less than 2 nm are called micropores and mesopores have diameters between 2 nm and 50 nm. The thickness of the inorganic backbone bridging the pores is so small that most of the matter is near the surface and “dangling” bonds are stabilized by OH groups or branches like -CH₂.

Water departure,



destroys the inorganic backbone and drives the crystallization-densification.²⁴⁻³¹ There is thus a relationship between the backbone composition, the hydroxyl content, and the meso/microposity (and hence between this porosity and the water



content) and the sintering temperature. The nanostructure and the porosity (and hence the densification and many other properties) can therefore be tailored by the chemical parameters controlling the inorganic polymerization and the hydroxyl content: relative proportion of reagents, additions of complexing liquids, temperature, sonification, sintering atmosphere, and heating rate.^{7,25,28,30–33} These remarks are general: for instance, the chain length of SiC (or C) polymeric precursor determines the silicon/carbon and carbon/hydrogen stoichiometry, because terminal branches contain more carbon and hydrogen.

Like many hydrates, gels present a unique challenge when densified under pressure at room temperature.^{34–37} Due to the liquid (water generally) present at the boundary, viscous rearrangement under pressure allows densification and optimization of the contact between polymeric grains, approaching the “perfect” packing obtained by sedimentation: true sintering can be achieved under the combined action of the pressure and the liquid phase soaked in the pores (water generally, but also alcohol). Gel sintering is associated with an increase in optical clarity.³⁶ On heating, the grains formed retain a memory of the packing of primary moieties. The grain growth does not destroy this arrangement. Figure 12.4b shows gel pellets of Nasicon solid solutions prepared by different sol-gel routes. Translucent or even optically clear samples are easily obtained. The plasticity of the gel offers the possibility of facilitating the compaction of any kind of particle, especially those with an elongated shape (whiskers, platelets), by coating each particle with a gel film.³⁷ The gel coating lubricates the particle and promotes homogeneity of the applied pressure. Plasticity and shapability disappear with the loss of the water adsorbed at the “grain” surface, above $\sim 200^{\circ}\text{C}$. Depending on the composition, the shrinkage rate then decreases up to 500°C (zirconia) to 1000°C (aluminosilicates), where drastic shrinkage takes place. The latter results from the backbone rearrangement due to the departure of the last stabilizing OH groups (Figure 12.2 and Figure 12.3). Note that because of the ability of the gel to be deformed, a memory effect very similar to the well-known paste memory of kaolin-rich porcelain paste can be observed. An example is shown in Figure 12.5, with a compacted pellet of zirconia gel fired at 1200°C .

Gels transform more or less gradually into a meso/microporous glass.^{24–26} A logarithmic plot of the weight loss vs. the inverse of the temperature allows the onset determination of water and hydroxyl departures, and hence the measurement

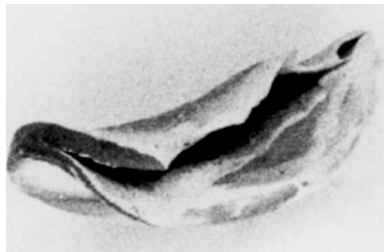


FIGURE 12.5 Self-wrapped zirconia pellet after firing at 1200°C (diameter ~ 10 mm).

TABLE 12.2
Gel Compositions, Specific Area and Hydroxyl Coverage Ratio for Some Heat-Treated Gels

Precursor	Thermal Treatment (°C)	Formula	Specific Surface Area (m ² /g)	OH(nm ²)
Aluminum butoxide	300	Al ₂ O _{2.5} (OH) _{0.9} 0.4 H ₂ O	530	8.8
	600	Al ₂ O _{2.8} (OH) _{0.35} 0.3 H ₂ O	350	5.5
Aluminum butoxide + silicon methoxide (1/1 molar)	400	Si ₂ Al ₂ O _{6.5} (OH) 1.2 H ₂ O	680	3.5
	600	Si ₂ Al ₂ O _{6.7} (OH) _{0.6} 1.9 H ₂ O	630	2.2
(1/2 molar)	400	Si ₂ Al ₂ O _{6.7} (OH) _{0.65} 0.9 H ₂ O	515	3.1

After Vendange, V., and Colomban, P., Determination of the hydroxyl group content in gels and porous “glasses” issued of alkoxide hydrolysis by combined TGA and BET analysis, *J. Porous Mater.*, 3, 193, 1996.

of x and m values in the gel formula.^{26,31} Measurement of the specific surface area by BET methods allows the calculation of the hydroxyl coverage ratio. Representative measured gel compositions are given in Table 12.2. The high value of the hydroxyl coverage ratio explains the high correlation between the hydroxyl group elimination and the nucleation-densification reaction.

Note that the high specific surface area of gels is not related to their apparent density, but to the intrinsic characteristics of the network. For instance, specific surface areas as high as $\sim 1000 \text{ m}^2 \cdot \text{g}^{-1}$ are achieved for optically clear gels prepared by slow hydrolysis (their density is close to 1.5 to $2 \text{ g} \cdot \text{cm}^{-3}$),^{31,33} but also for aerogels made through supercritical drying³⁸ and for gels obtained by oxyhydration of aluminum in the presence of mercury (the apparent density of these last materials is approximately $0.05 \text{ g} \cdot \text{cm}^{-3}$).³⁹

B. SINTERING

It is well established for “usual” ceramics processed from crystalline powders that the denser the material in the green state, the better the densification. However, although sol-gel prepared nanosized powders have been available for many decades, their ease of use is more recent. In the 1970s, poor density was generally obtained with gel powders because many engineers overheated them before compaction in order to develop their crystallinity. This thermal treatment drastically decreased their ability to sinter. When a gel is converted by thermal treatment into a meso/microporous xerogel (also called “porous glass”) above approximately 400°C , OH/H₂O loss and squeezing of the (Si-O)_n network occur. This first step in shrinkage (Figure 12.2) related to the gel densification was

suppressed. Consequently the gel plasticity disappeared. The presence of some M-OH “dangling” bonds in place of M-O-M bridges stabilizes the surface of the porous network, which makes the densification sensitive to the atmosphere (H_2 , H_2O , vacuum or air).^{26,27} Densification and nucleation for refractory or glass-like compositions result from the short range structural rearrangement induced by surface dehydroxylation at a temperature of about $0.5 T_m$ (melting temperature).^{1,36} It can be compared to the $0.8 T_m$ value usually required for the sintering of a fine ceramic powder. There is thus a direct relationship between the hydroxyl content, the composition, and the meso/microporosity of a (xero)gel. A thermal treatment above the crystallization step leads to a powder which has lost its sinterability: the grain surface has been smoothed, which hinders the sintering at the temperature expected compared with ball-milled powders of the same grain size. The nanostructure and the sinterability can therefore be tailored by the chemical parameters controlling the inorganic polymerization and the hydroxyl content (relative proportions of reagents, addition of complexing liquids, temperature, sonification, sintering atmosphere, etc.). In the case of glass-forming compositions, a viscous sintering may occur while the dehydroxylation-densification proceeds.^{1,40} In this case, bloating can be observed if gas departure (H_2O from dehydroxylation, CO_2 from oxidation of unhydrolyzed organic branches) is hindered up to a viscous state, allowing the formation of bubbles.

Convenient sol-gel processing, compaction, and firing allow the synthesis of optically clear ceramics. Two examples are presented in Figure 12.6, a ferroelectric PLZT 65/35 ceramic prepared by hybrid sol-gel route⁴¹ and a mullite matrix prepared using aluminum-silicon ester and silicon-methoxide.²³ Note the opaque skin around the transparent PLZT ceramics is related to PbO loss. When a partial pressure higher than the equilibrium pressure required to avoid any PbO excess

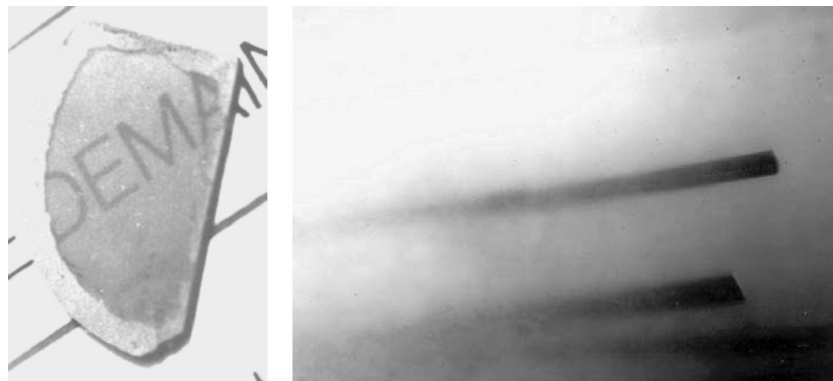


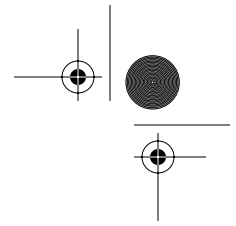
FIGURE 12.6 (a) Optically clear PLZT 65/35 ceramic sintered in PbO-enriched atmosphere (thickness ~5 mm). (b) Translucent mullite ceramic with SiC fibers (diameter $12 \mu\text{m}$).



at the grain boundaries in the bulk is used, it gives a red shade to the yellow-colored optically clear ceramic.

C. MULTICOMPONENT MATERIALS

For a long time, the use of polymeric and sol-gel precursors was limited to simple compositions: SiO_2 , TiO_2 , ZrO_2 , etc. The main difficulty in multicomponent and nonstoichiometric materials is to achieve the right composition. This requires the precise determination of the elemental composition of liquid precursors or reagents and to take into account any loss related to the various transformation rates, volatility, polycondensation, or even some polymerization.^{1,2,6,7,42-45} For instance, aluminum alkoxides are very hygroscopic (instant hydrolysis with water traces), whereas tributylphosphate can stay months in humidity without hydrolysis. Some reagents are volatile (e.g., many methoxides). Consequently the hydrolysis of a mixture of reagents could give local heterogeneities. During the drying of gels containing elements that do not participate in the polymeric network (e.g., alkali ions), they migrate to the evaporation front and the gel (and container) surfaces have higher concentrations of these elements. This problem was first encountered (and solved) at the very beginning of the sol-gel history for the synthesis of PLZT (optically clear ferroelectric ceramics made of lanthanum lead zirconate-titanate)⁴¹ and then NASICON (a solid solution of sodium zirconium phosphate-silicate solid electrolytes).^{6,7} The proposed solutions were (1) to use reagents in which both elements link early [e.g., the aluminum-silicon ester $(\text{OC}_2\text{H}_5)_2\text{-Al-O-Si}(\text{OC}_2\text{H}_5)_3$ has intermediate behavior between pure aluminum butoxide and silicon ethoxide].^{16-18,44-46} Controlled hydrolysis is thus very easy and catalysis is not required, as for the hydrolysis of silicon-alkoxides; (2) to use an inert reagent (propanol, hexane) as a solvent for the alkoxide mixture in order to control the hydrolysis by water diffusion;^{6,7,45-52} (3) to increase the chain length of the most hygroscopic reagent in order to slow down its hydrolysis rate; (4) to use hybrid methods: only the gel formers (silicon, aluminum, zirconium, titanium, phosphorus, germanium, etc.) are used in the form of alkoxides, the elements to be present as ions in the gel (sodium, lithium, lead) being added in the water used to hydrolyze the gel formers, or even as a solid powder.^{1,6,41,47} A good example was proposed for the synthesis of PLZT: zirconium and titanium alkoxides are first mixed with propanol to obtain a very good dispersion of zirconium and titanium elements, a very important characteristic for the final ferroelectric and optical properties.^{41,53,54} Lead oxide powder is then mixed to the alkoxide alcoholic mixture and hydrolysis is provoked with an aqueous solution of lanthanum acetate (acetic acid dissolving the lead powder). Lead oxide gives rise to a liquid phase at relatively low temperature, and fast diffusion of Pb^{2+} ions takes place before the melting temperature; with such fast diffusion of ions, any heterogeneity will rapidly disappear on heating. Thus, in hybrid routes, the use of sol-gel or polymeric precursors has to be limited to the elements with the lowest diffusion coefficients. In this way it is possible to prepare better materials at lower cost.



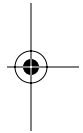
IV. COMPOSITES AND MULTIPHASE MATERIALS

A. PARTICULATE-REINFORCED MATERIALS

The “simplest” application of sol-gel materials is as abrasive grains. Abrasive particles can be dispersed into vitrified or resin-bonded grinding wheels, coated abrasive belts, sheets, and discs. In 1981, 3M Company introduced the first sol-gel abrasive particle, referred to as Cubitron, in the Regal-coated abrasive fiber disc product line.⁵⁵ The idea to use sol-gel processing originated from the processing route of ceramic fibers developed at 3M by Sowman⁵⁶ some years before. Commercially available boehmite (AlOOH) sol is derived from the hydrolysis of aluminum alkoxide, a by-product of the Ziegler process for the production of long-chain alcohols. When a metal salt is added to the boehmite sol, it provokes gelation and a stiff gel is formed. Afterwards this gel is dried, crushed, and screened to the appropriate size distribution, calcined, and then sintered at a temperature between 1200 and 1600°C. The resulting material is screened and ready to be used as an abrasive particle.

Nonoxide ceramics are finding increasing applications as high-speed cutting tools for metals.⁵⁷ The combination of sol-gel processing and reaction-sintering has been used to prepare dense nonoxide abrasive grit.⁵⁸ An Al_2O_3 sol was prepared by dispersing boehmite powder into HNO_3 containing water heated to $\sim 80^\circ\text{C}$. The sol was seeded with $\alpha\text{-Al}_2\text{O}_3$ crystallites. The abrasive grains were prepared from the dispersion of carbon black and TiO_2 in the seeded Al_2O_3 sol. Glycerol was added to prevent oxidation of the carbon black during calcination. The gel was dried, crushed, screened, and calcined at 1000°C and then thermally heated to 1400°C and then to 1900°C under a flowing N_2 atmosphere for the formation of TiN and AlN by carbothermal reduction. The final microstructure (AlN/TiN/AlON) is controlled by the amount of TiO_2 in the sol and by the carbon content. The great advantage of sol-gel abrasive particles is the ability to introduce chemical changes, which modify the alumina crystal structure and enable the optimization of grinding.

Particulate reinforcement (platelets and whiskers) is used to improve the toughness of small shaped pieces or to facilitate machining. This type of reinforcement is also used to increase the toughness of monolithic ceramics and of the matrix of fiber-reinforced composites. Figure 12.7a shows an example application, a dispersion of submicronic zirconia in a mullite matrix in between woven SiC fibers. Another example application is the “machinable” sol-gel prepared mica-ceramic composite that can be cut by a conventional metallic saw⁵⁹ and is used as an insulating material for precision machines and as a substrate for electronic parts. The homogeneous dispersion of anisotropic particles in a powder and the compaction of the resulting mixture are always difficult because the applied load decreases with the number of contact points. The use of liquid aids (colloidal processing) counteracts this drawback, although imperfectly. Gel embedding offers a new route for the mixing of powders and particulate reinforcements due to the incorporation of a viscous substance, the reactivity of which can be tailored by compositional design.³⁷ Cold molding makes it possible to prepare shaped and crack-free pieces. The process is the following: powder and



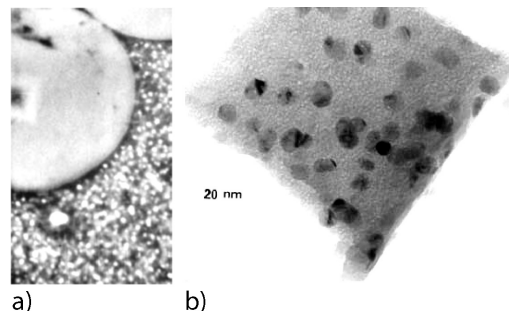
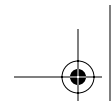


FIGURE 12.7 (a) Scanning electron micrograph (SEM) of a mullite matrix CMC reinforced with submicronic zirconia (fiber diameter 12 μm). (b) TEM of a cobalt dispersion in an aluminosilicate matrix synthesized by the infiltration- H_2 firing route.⁸⁷

particles are dispersed together in an anhydrous solvent (e.g., propanol) before the addition of alkoxides. After mixing, pH-controlled water is poured in under vigorous mechanical stirring, which has to be maintained until a paste of thick consistency is obtained. The paste is then dried to give a flour-like powder. The powder is compacted and sintered. Gel embedding promotes a homogeneous load/pressure transfer and hence suppresses the densification hindrance induced by the platelet addition. For example, zirconia gel embedding of the mullite powder increases the microhardness by 30% and the toughness by 40%. The combination of zirconia gel embedding and platelets addition increases the K_{IC} value to about 5 $\text{MPa}\cdot\text{m}^{1/2}$.³⁷

B. METAL- AND CERAMIC-CERAMIC NANOCOMPOSITES

Metal-ceramic microcomposites (cermets) have been prepared for a long time, especially by dispersion of nickel particles in a silica matrix. Metal nanocomposites (iron, nickel, tin, and copper particles in a silica or alumina matrix) have been prepared by different groups.⁶⁰⁻⁶⁴ More complex materials with nanodispersion of pure or alloyed iron, cobalt, and nickel in aluminosilicate matrices have also been prepared.^{65,66} The main methods can be classified as follows: (1) the mixing of the (sub)micronic metal powder within a liquid matrix precursor; (2) the mixing of the alkoxides with an aqueous solution of metal ions and controlled H_2 reduction on firing; and (3) the preparation of a porous host matrix impregnated by a concentrated solution of transition metal nitrates and controlled reduction. Homogenous dispersions are achieved at the submicronic scale (Figure 12.7b). About 5% of matter in volume (15% in weight) can be incorporated in one cycle of impregnation/firing. The metal content can be increased by successive impregnation-firing cycles (up to ~50% in volume). Combined infiltrations with different metal and alloy precursors can tailor the magnetic and electromagnetic properties, in particular the microwave absorption between 0.1 and 10 GHz.⁶⁶ These new materials can find applications at higher temperatures, as their magnetic properties are maintained up to 550°C.

The preparation of ceramic (oxide-oxide, carbide-carbide, etc.) nanocomposites is also rather old and many authors have reported some exceptional properties.^{49,50} This field of study developed rapidly. It is clear that more work is needed in order to further understand the mechanics of nanocomposites.

C. ONE-DIMENSIONAL AND TWO-DIMENSIONAL FIBER-REINFORCED COMPOSITES

One of the main problems in the preparation of ceramic matrix composites (CMCs) is achieving a low open porosity in the matrix in order to protect the fiber from the environment and to optimize the mechanical strength and toughness. Fibrous fracture of CMCs is mandatory to get a stable and reliable strength value to be used for parts design. In the case of weavable fibers forming a yarn, the interfiber voids are a few microns or less in size, which makes infiltration of liquid or gaseous precursors mandatory.^{12,23,67} In many cases, interyarn voids (1 to 100 mm³) of textile preforms are accessible only through interfiber voids close to 1 to 5 μm . Chemical vapor infiltration (CVI), a method based on the infiltration of gaseous precursors, is more expensive because of the duration of the synthesis cycle and the need for specific tools for each cycle.^{68,69} Furthermore, gaseous precursors are not well suited for the multicomponent oxide compositions required for functional composites. The presence of long-fiber geometrically invariant reinforcement inhibits the coherent shrinkage of the matrix. In the case of one-dimensional or two-dimensional (textile) reinforcements, this phenomenon can be solved by hot-pressing: the in-plane shrinkage can be counterbalanced by the thickness reduction if a viscous behavior is achieved during the hot-pressing.⁶⁷ A flowchart for this process is summarized in Figure 12.8.

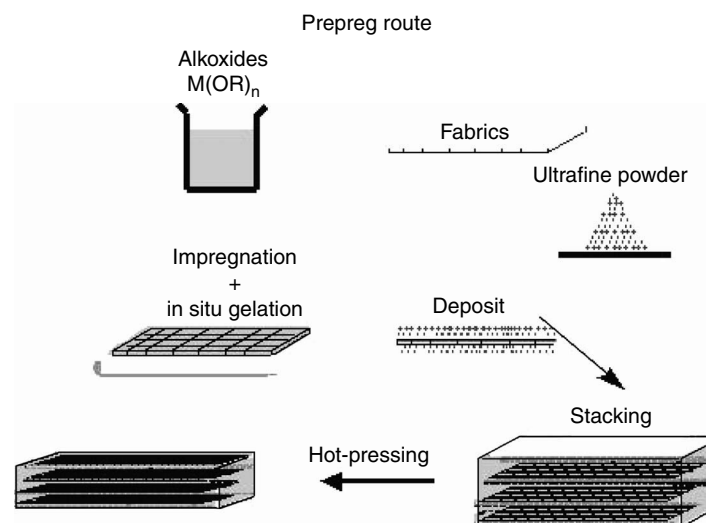
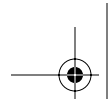


FIGURE 12.8 Schematic of the sol-gel process for the fabrication of woven fabrics reinforced CMCs.⁸⁷



Many attempts to prepare dense ceramic matrix composites by sol-gel methods have been made. A lot of them used mullite as the matrix material because of its excellent high-temperature strength and creep resistance, good chemical and thermal stability, low thermal expansion coefficient, and low permittivity. First, Qui and Pantano,⁷⁰ Pannhorst et al.,⁷¹ and then Russell-Floyd et al.⁷² demonstrated that sol-gel processing can be used. A group from Sheffield⁷³⁻⁷⁵ pointed out that highly densified unidimensional continuous carbon fiber-reinforced mullite composites could be successfully prepared by a single-stage infiltration process, using Ludox[®] colloidal silica sol (Dupont AS40) and α -alumina powder (A1000G, Alcoa), followed by hot-pressing. The pH of the Ludox[®] sol was adjusted to 2 to 3 before dispersion of alumina powder.

Composites reinforced with woven (carbon, SiC, or oxide) fibers could be successfully prepared by a two-step process,⁷⁶⁻⁸¹ as illustrated in Figure 12.8. First the fibers of a two-dimensional woven fabric are impregnated with a liquid alkoxide mixture (for instance, a mixture of zirconium-*i*-propoxide, aluminum-silicon ester, tributylborate and germanium propoxide for mullite matrix composite), which fills in the voids between the fibers, *in situ* transforms into a gel by reaction with atmospheric moisture and is to be converted into a (glass-) ceramic by pyrolysis during the hot-pressing step. Before pyrolysis, a fine amorphous matrix precursor powder, suspended in chlorobenzene, is deposited onto the layers of woven fiber fabric (prepreg textile). This matrix precursor powder is prepared by rapid hydrolysis of the appropriate mixtures of alkoxides in propanol. The resulting gel is dried at about 750°C to drive most of the water and part of the hydroxyl groups out and thus reduce the subsequent shrinkage of polymeric oxide network. Then the doubly impregnated layers of textile fabric are stacked together in a graphite mold and hot-pressed at temperatures between 1000 and 1400°C. Below 300°C, gel viscosity promotes homogeneous pressure application. A liquid sintering aid (for instance, B₂O₃ or GeO₂) obtained by pyrolysis of appropriate gel precursors can be incorporated.⁷⁶⁻⁷⁸ Then the liquid sintering aid is eliminated either by incorporation into the matrix or by volatilization. Therefore it does not contribute to the formation of second phases at the grain boundary and does not decrease the thermal stability of the composite significantly. The dwell temperature is related to the composition of the matrix and of the interphase precursor. The transient liquid phase acts both to densify the matrix (sintering aid) and to maximize the contact between the grains of the matrix precursor during the hot-pressing step. Some examples of sol-gel fiber coating are a zirconia deposit on SiC fiber reinforcing a glass-ceramic matrix processed by the melt-infiltration technique (Figure 12.9a) and the SiC-coating interface in SiC-reinforced mullite matrix composite (Figure 12.9b).

D. THREE-DIMENSIONAL FIBER-REINFORCED COMPOSITES: NEAR NET-SHAPE SINTERING

For continuous three-dimensional fiber-reinforced bodies, the idea of using liquid ceramic precursors for the impregnation of the fibrous preform originates in the



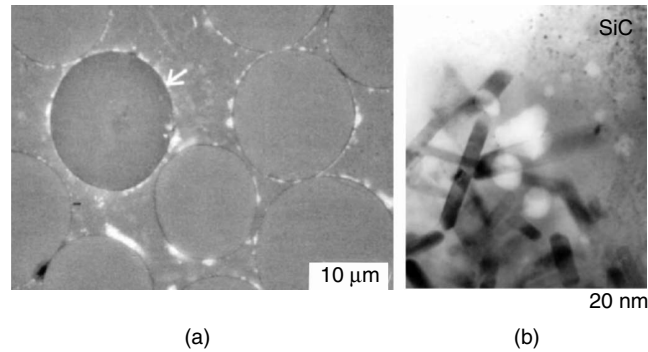
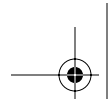
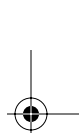


FIGURE 12.9 (a) SEM of a sol-gel ZrO_2 coated SiC fiber reinforced glass-ceramic. (b) TEM detail of the SiC-mullite coating interface; see the elongated mullite crystals ($l = 5\text{--}10$ nm).

preparation of carbon/carbon composites by pitch or phenolic resin infiltration.²³ To mimic this route, the slip-casting of a submicronic powder has been proposed,⁸² but this led to highly porous samples (open porosity close to 35 to 40%) exhibiting very poor mechanical properties and low protection of the fibers against corrosive atmospheres. Also, the range between the consolidation temperature and the temperature at which the matrix shrinkage leads to matrix cracking, within the geometric invariant preform or fabric, is small. Due to the fact that the achievement of a zero-porosity matrix is unrealistic for thermostable three-dimensional reinforcements (fabrics, felts, etc.), we will consider methods for increasing the mechanical strength of a porous body. The first idea is to avoid cracks, maintaining a coherent matrix (maximization of the number of interparticulate bonds without shrinkage), the second one is to improve the strength of the interparticulate bonds and/or of the intergranular phase (maximization of the reaction between grains), and the last one is to introduce between a phase between the grains, which hinders the shortening of the distance between their centers.

The first requirement can be obtained by filling the voids between slip-cast grains with a ceramic precursor, which, after a thermal treatment, is transformed into a refractory phase. The resulting intergranular phase may form an inert barrier between slip-cast grains and thus put the shrinkage off to higher temperatures.^{12,83} The mean size of alumina particle is $0.6\ \mu\text{m}$, which is allowed to pass through interfiber voids. Thermal treatment at 1000°C was carried out in order to initiate the consolidation of the matrix without developing significant shrinkage of alumina grains.

Figure 12.10 shows a schematic of the two-step infiltration process.²³ The first step consists of the preparation of a powder compact within the fiber preform by a routine slip-cast infiltration, the body being dried, and then strengthened by heating at a temperature close to the onset of shrinkage. The second step consists of the infiltration of the strengthened body by a liquid (polymeric) precursor that is first converted into a solid (a gel by reaction with water or diols if alkoxides are used^{23,77,83,84}), or by the action of oxygen if polyvinylsilane (PVS) is used to



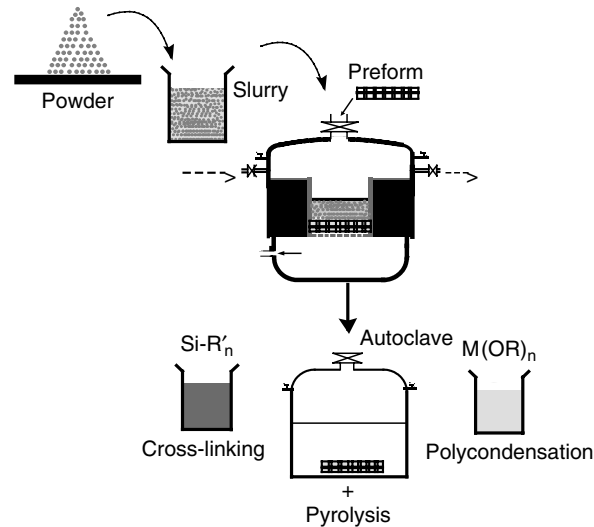


FIGURE 12.10 Schematic of the oxide (alkoxides) or nonoxide (polymers) matrix precursors infiltration for fabricating three-dimensional reinforced composites. (After Reference 87.)

prepare SiC matrix,⁸⁵ and then, during pyrolysis, into a refractory intergranular phase. This second step can be repeated as many times as necessary to optimize the interparticle bonding.

As explained in the previous part, optimization of the microstructure might involve (1) an increase in ceramic yield by the pyrolysis of the precursor, (2) an increase in thermostability of the resultant phase, in order to limit the shrinkage of the refractory interphase and postpone the whole matrix shrinkage toward higher temperatures, or (3) the optimization of the fiber-matrix interface. For instance, various polymeric precursors can lead to inert, refractory, and nonreacting interphases: zirconium-*i*-propoxide as zirconia precursor, aluminum-*n*-butoxide as alumina precursor, lanthanum-alkoxide, and homologues as rare earth oxide precursors. Sometimes titanium-*i*-propoxide, tetraethoxysilane, and aluminum-silicon ester can be used as rutile, silica, and aluminosilicate precursors, respectively. These last three compounds, which slightly react with many oxides, might also be used to strengthen the interparticle bonds. It is very important, however, to simultaneously maintain a net-shape sintering behavior. The room-temperature and high-temperature flexural strength was increased after five (Figure 12.11) cycles of postinfiltration *in situ* hydrolysis-polycondensation and 1000°C heating, zirconium-*i*-propoxide being used for the first four cycles and aluminum-silicon ester for the last one.^{12,83} Confirmation was given by tensile test, at room temperature. The increase in mechanical strength arises from the filling of the voids (porosity decreases), but also from the blocking of shrinkage due to the zirconia “inert” phase. The high stability of zirconia coatings has been used in many oxide-oxide composites. The addition

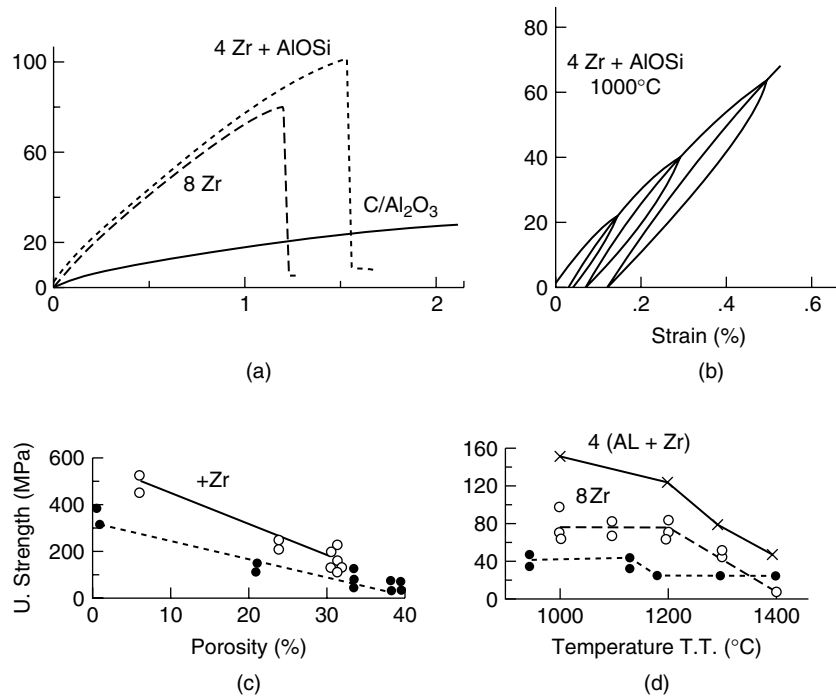
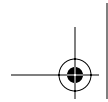


FIGURE 12.11 Improvements of the mechanical properties of three-dimensional reinforced CMCs by hybrid infiltration routes: (a) R.T. flexural stress-strain plots for a three-dimensional carbon fiber reinforced composite before and after cycles of infiltration (comparison between eight cycles with zirconium propoxide and four cycles plus a last infiltration with aluminum-silicon ester); (b) plot of the mechanical strength as a function of the final open porosity for composites and matrix of equivalent porosity, before and after infiltration (Reprinted from Colomban, P. and Wey, M., Sol-gel control of the matrix net-shape sintering in 3D reinforced ceramic matrix composites, *J. Eur. Ceram. Soc.*, 17, 1475, 1997. With permission from Elsevier); (c) R.T. tensile behavior; (d) comparison of the R.T. mechanical strength after thermal treatments at various temperatures. (Reprinted from Colomban, P., Tailoring of the nano/microstructure of heterogeneous ceramics by sol-gel routes, *Ceram. Trans.*, 95, 243, 1998. With permission from The American Ceramic Society.)

of aluminosilicate precursor for the last infiltration strengthens the bridge between particles and decreases the open porosity. Tensile measurements show that the mechanical properties achieved through the oxide route are very similar to those of the usual SiC made by the CVI process, although the matrix Young's modulus is lower in the former (30 GPa instead of 75 GPa for the CVI SiC matrix). A rather pronounced hysteresis in loading-unloading cycles is observed. The same behavior is observed for composites prepared by combining SiC powder and PVS infiltration.^{23,84}



Alloying the materials obtained from liquid precursors offers a new route to create particular micro/nanostructures in order to optimize the properties of porous materials.

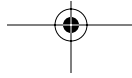
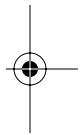
E. FUNCTIONALLY GRADED MATERIALS

By selecting the appropriate sol-gel precursors, the dwell temperature required to achieve maximum densification can be raised or lowered by about 100°C.^{1,36} This makes it possible to combine several kinds of impregnated fiber/matrix interphases in the same composite in order to tailor its physical and/or chemical properties for a particular application. Composites have been fabricated that combine various kinds of woven fibers (SiC Nicalon®, Nextel®, Almax®, Saphikon®) with various kinds of matrices (LAS, mullite [a pure dielectric with a real microwave permittivity close to 5 at 10 GHz], Nasicon [a solid electrolyte with the structural formula $\text{Na}_{1+x}\text{Zr}_2\text{Si}_x\text{P}_{3x}\text{O}_{12}$ ($0 < x < 3$) offers the advantage of an electrical conductivity varying by four orders of magnitude as a function of x], celsian [a corrosion-resistant ceramic], zirconia)^{6–10,76,78,79,86,87} in order to tailor thermomechanical and electromagnetic properties simultaneously.

The processing can be summarized as follows: The fibers of a two-dimensional woven fabric are first impregnated with a liquid alkoxide mixture, which fills the voids between the fibers, transforms *in situ* into a gel by reaction with atmospheric moisture, and will be converted into a (glass)-ceramic by pyrolysis during the hot-pressing of prepreg fabrics covered with the matrix powder precursors. Depending on both the matrix and the fibers, several different “interface precursors” can be used, either alone or in various combinations. Finally, the doubly impregnated, coated woven fabrics are stacked in a graphite mold and hot-pressed, typically between 950 and 1400°C. By selecting the appropriate sol-gel precursors, the dwell temperature required to achieve maximum densification can be raised or lowered by about 100°C. This makes it possible to combine several kinds of fiber-reinforced layers in the same composites in order to tailor, unidirectionally, the microwave absorption along the direction perpendicular to the body. Examples given in Figure 12.12 show (1) a composite consisting of a zirconia matrix and a mullite matrix, both reinforced by SiC Nicalon NLM 202 fibers (4 + 4 layers), and (2) NASICON matrix composite reinforced on one side by low-permittivity Nextel mullite woven fibers (4 layers) and on the other side by conducting Nicalon SiC woven fibers (2 layers).

V. CHARACTERIZATION OF MULTIPHASE MATERIALS

One of the difficulties in the characterization of multiphase materials is the need to analyze the different phases at various scales: at the scale of each phase, at the scale of their association (interfaces and intrafaces), and at the scale of the parts. We will address two methods, which can be used very rapidly for this type



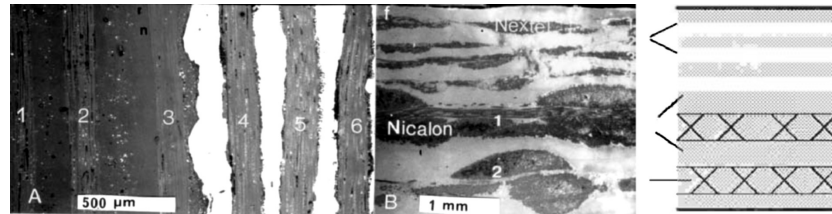


FIGURE 12.12 Examples of FGM CMCs: (left) the combination of NLM Nicalon SiC fiber reinforced zirconia (in white) and mullite (in black) matrices; (right) a Nasicon matrix reinforced with mullite (Nextel) and SiC (NLMTM) fibers (see the sketch). (Reprinted from Colomban, P., Process for fabricating a ceramic matrix composite incorporating woven fibers and materials with different compositions and properties in the same composite, *Mater. Technol.*, 10, 89, 1995. With permission.)

of study. Both methods are associated with optical microscopes, which provides easy analysis of regions ranging in size from a few square centimeters to $1 \mu\text{m}^2$.

A. DEPTH-SENSING MICROINDENTATION

The measurement of local mechanical properties is an important step in understanding of the macroscopic behavior of multiphase materials. The indentation hardness test is probably the simplest method of measuring the mechanical properties of materials. Figure 12.2b shows the evolution of the microhardness as a function of the thermal treatment temperature of a Nasicon sample. The use of load-controlled depth-sensing hardness testers which operate in the (sub)micron range enables the study of each component of the composite more precisely.

Following the work of Loubet et al.,⁸⁸ Young's modulus (E) and Vickers' microhardness (H_v) can be extracted from the unloading part of load-displacement plots by considering the different contributions of the elastoplastic behavior of the indented materials. Figure 12.13a shows a schematic of an indentation test and Figure 12.13b gives the corresponding curves of loading and unloading versus in-depth penetration. For materials with high plasticity, the remnant penetration depth of indentation (h_p) is close to h_e , given by the intersect of the initial unloading step tangent with the x -axis; for plastic material $h_p = h_{\text{max}}$. The area delimited by loading and unloading curves is proportional to the work of indentation. On the other hand, the hysteresis is very small ($h_p \ll h_e < h_{\text{max}}$) for densely packed structures and high Young's modulus phases (e.g., SiC and sapphire). The slope of the straight line is directly related to Young's modulus:

$$\left(\frac{1-\nu^2}{E} + \frac{1-\nu_0^2}{E_0} \right)^{-1} = \frac{dF}{dh} 4\sqrt{\pi} (h_p \tan \theta)^{-1} \quad (12.5)$$

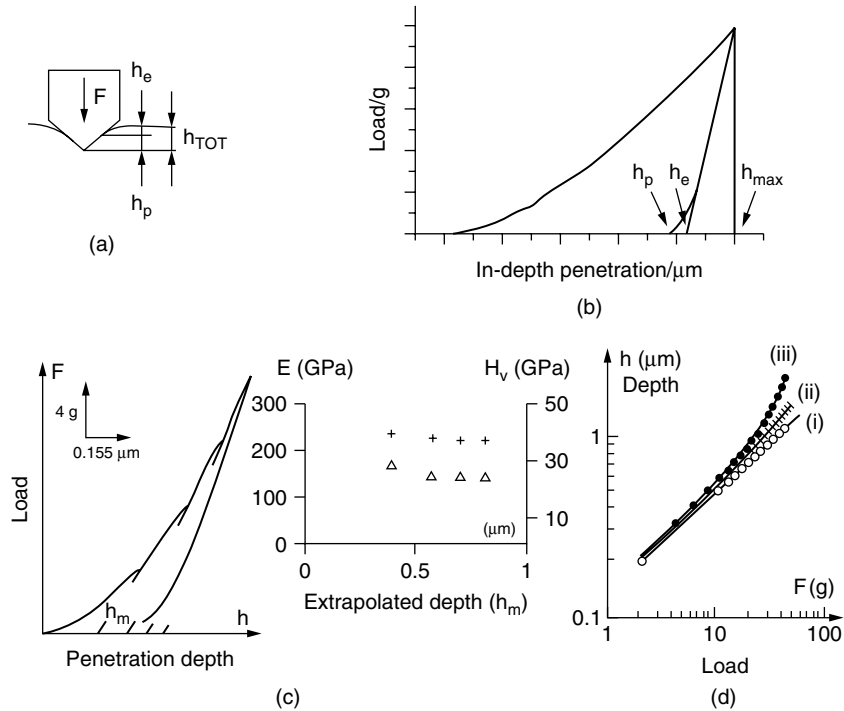
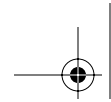
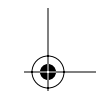
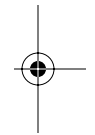
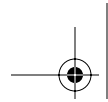


FIGURE 12.13 (a) Sketch of the indenter penetration in a ceramic and (b) corresponding loading-unloading plot. (c) Example of the partial unloading from which the Young's modulus and microhardness are extracted. (Reprinted from Colomban, P. et al., Sol-gel mullite matrix-SiC and -mullite 2D woven fabrics composites with or without zirconia containing interphase. Elaboration and properties, *J. Eur. Ceram. Soc.*, 16, 301, 1996. With permission from Elsevier.) (d) Comparison of the logarithmic plots for indented fibers in their matrix: a fiber sliding is observed for fibers (ii) and (iii).

where dF/dh is the slope of the curve, h_p is the plastic penetration, θ is the half angle of the Vickers' pyramid faces, E , ν , E_0 , ν_0 , being the Young's modulus and the Poisson's coefficients of the material and the indenter, respectively. The observation of noise and kinks on the loading/unloading curves is related to the formation of cracks. Young's modulus is measured for the constant regime observed for a set of indentation under different loads. Partial unloading (see Figure 12.13c, where three partial unloadings have been made before the load has been removed) is sufficient to extract the hardness, H_c , value used for the calculation.^{37,78,89} Recent homemade or commercially available instruments allow the study of submicronic regions (nanoindenters). This method is well-suited to analyze the various phases and allow the study of the gel-ceramic transformation. Indentation of a fiber, its coating, or the matrix allows one to observe the evolution of the material as a function of processing and thermal aging. Note that if the applied load exceeds

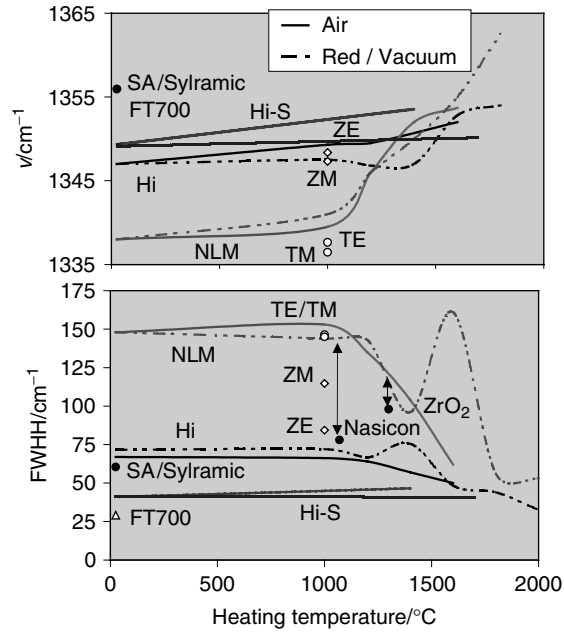




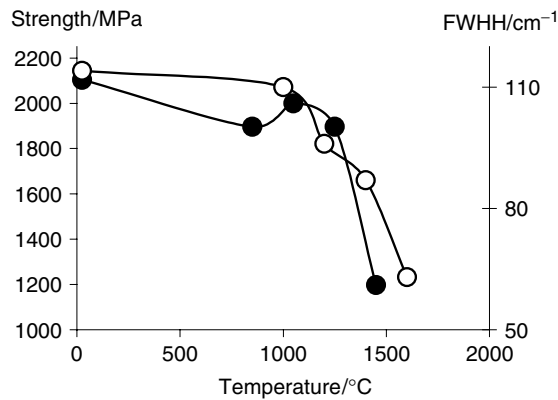
the threshold load (F_s), the fiber slides within the matrix and a step becomes visible at the fiber periphery: after indentation, part of the fiber push-down is permanent (Figure 12.9a). This makes it possible to study the departure of the fiber/matrix mechanics from the linear behavior on logarithmic plots of the in-depth penetration as a function of the applied load. This gives evidence of the fiber sliding in its matrix (Figure 12.13d). The high strength and toughness of (glass)-ceramic matrix composites directly result from the low fiber-matrix bonding originating in the processing. This interphase acts as a “fuse,” deflecting the matrix microcracks parallel to the fiber axis and thus avoiding the early failure of the fibers. This interphase is formed *in situ* during the hot-pressing as a result of the fiber-matrix chemical reaction or results from the deposit of a thin coating of carbon, BN, SiC, ZrO₂, etc.,^{23,78,90,91} when nonreactive matrices are used. An important parameter to be controlled is the sign and the level of the residual mechanical stresses in the composite arising after processing from the mismatch of fiber (coating) and matrix (substrate) coefficients of thermal expansion. The sliding strength is usually measured on one-dimensional composites using instrumented or noninstrumented microhardness testers following different models.^{92,93}

B. MICRO-RAMAN SPECTROMETRY

Routine x-ray diffraction techniques fail to analyze nanosized/nanocrystalline materials: small size effect and short-range disorder are hardly distinguished and long counting times are required. On the contrary, Raman spectroscopy has demonstrated its capability to analyze low crystallinity and amorphous materials. Covalent-bonded materials are well-suited systems for Raman analysis. Their spectra are easily understood with the molecular model (the vibrational unit is built with the stronger bonds of the unit cell). However, their spectra do not change very much with “particle” size. On the contrary, because of long-range Coulomb interactions, spectra of ionocovalent structures are very sensitive to particle size, but can be understood with the molecular model. Thus Raman parameters (peak intensity, wave number, bandwidth, and shape) are very sensitive to any change of the chemical bonds: length, strength, geometry, etc. An example is given in Figure 12.14a with the plot of the wave number and bandwidth of the main Raman peak of disordered carbon (sp^{2/3} hybridized C–C bond) for different SiC fibers (NLMTM, HiTM, and Hi-STM from Nippon Carbon; TMTM, TETM, ZMTM, and ZETM from Ube Industry; and SA[®] from Sylramic) as a function of their thermal treatment in different temperatures and atmospheres.^{94–97} Modifications induced by contact with a ceramic matrix or a coating can also be considered. Most of the properties controlled by the particle size (electrical conductivity, mechanical strength; e.g., in Figure 12.14b) are correlated to Raman parameters, which conversely can be used to predict these properties.

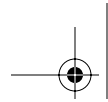


(a)



(b)

FIGURE 12.14 (a) Plot of the wave number and bandwidth (full width at half height) of the sp^{23} C–C raman peaks for different SiC fibers after various thermal treatment in air or in nonoxidizing atmospheres. (b) Comparison between ultimate tensile strength and sp^{23} peak FWHH as a function of thermal treatment for SiC Hi Nicalon fibers. (Adapted from Colombari, P., Raman microscopy and imaging of ceramic fibers in CMCs and MMCs, *Ceramic Trans.*, 103, 517, 2000. With permission.)



1. The Raman Effect in Nanomaterials

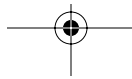
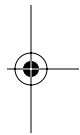
First, Raman spectroscopy has an intrinsic “nanospecificity” since the probes are the (ionocovalent) bonds themselves. The study of extended domains includes nanodomains also (the volume probed by the spot determines how many). Using the molecular description, the vibrational atomic unit is the “molecule” found in the structure when considering only the strongest covalent bonds between metal cations and oxygen (or carbon, nitrogen, etc.) anions. Repetition of this vibrational unit must give the whole structure, like for the unit cell in crystallography. Stretching modes are characteristic of the chemical bond and allow for composition identification. Bending modes are more sensitive to the neighboring entities and hence to the short-range order. Vibrational and external modes, which correspond to the relative motions of the vibrational units, depend on the structure. Roughly speaking, Raman spectra are the projection of all the vibrations on the energy axis. Structures made of well-defined covalent vibrational units will give nice sharp peaks, whereas broad bands will indicate that different configurations and/or many electric or atomic defects exist in the material.

If the proportion of atoms belonging to the (near) surface region is significant (Figure 12.15a), the disorder related to the various atomic arrangements will contribute to Raman features.^{94–102} We can say empirically that the chemical bonds located as far as 5 atomic distances (the approximately 1 nm short interaction length expected for covalent-bonded materials) or even 15 atomic distances (the long interaction length of approximately 3 nm expected for ionocovalent structures) from the skin atoms have a state different from those in the bulk. It is obvious that vibrational properties of surface atoms will dominate the spectra for a grain size of less than 20 nm (1 nm interaction length) or less than 50 nm (3 nm interaction length).

2. Correlation Between Raman Parameters and Grain Size

Many techniques for the preparation of nanosized materials (sol-gel, thermal treatment of polymeric precursor, electrochemical deposition, atomic layer deposition [ALD], etc.) lead to amorphous or low-crystallinity compounds by quenching of a liquid-state local structure or a very disordered state. At a given temperature, two phenomena can be at the origin of the broadening of the Raman spectrum: (1) the loss of periodicity because of the large contribution of surface atoms, and (2) a low crystallinity, that is to say, short-range disorder or bond distortion. In many cases the exact origin is not obvious and a comparison must be made with TEM.¹⁰²

Different models have been used to derive the particle size from Raman spectra^{90,96,99–105} As an example, we shall briefly explain the phonon confinement model (PCM). The scattering of one photon by n phonons is governed by the momentum conservation. Only vibrations from the center of the Brillouin zone (BZC) should therefore be active in one phonon process (first-order Raman spectrum) and this is actually the case in large and flawless crystals, where



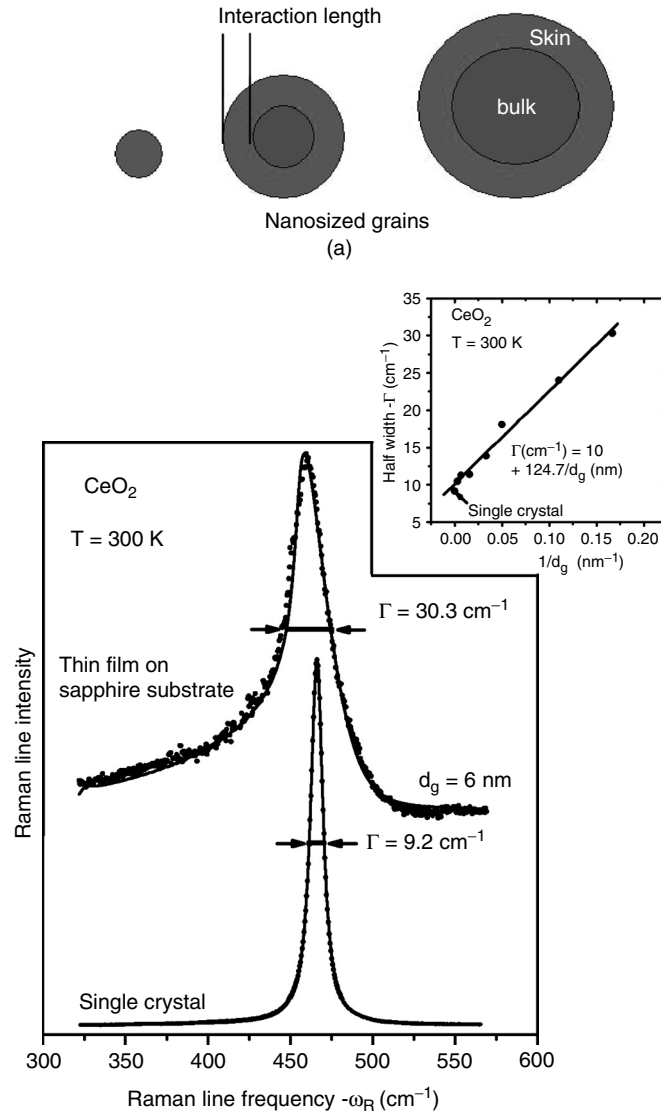


FIGURE 12.15 (a) Comparison of the relative proportion of skin and bulk atoms in nanosized grains for a given interaction length. (Reprinted from Colomban, J., Raman analysis and “smart” imaging of nanophases and nanosized materials, *Spectroscopy Europe*, 15, 8, 2003. With permission from Wiley.) (b) Comparison of the Raman spectra of CeO_2 in a single crystal and in a nanocrystalline ceramic (6 nm grains). Note the plot of the half width as a function of the inverse grain size. (Reprinted from Kosacki, I. et al., Raman scattering and lattice defects in nanocrystalline CeO_2 thin films, *Solid State Ionics*, 149, 99, 2002. With permission from Elsevier.)



phonons virtually propagate to “infinity.” However, short-range disorder, bond distortion, or nanocrystallinity can destroy periodicity and confine the phonons spatially. This introduces an uncertainty on k (the selection rule is broken by crystalline imperfection), and because dispersion curves are not symmetrical with respect to BZC, the “sampling” of k -space provokes band shifting and asymmetry. In the first approximation, Raman line broadening can be described by the (linear) dependence of its half width upon the inverse grain size (Figure 12.15), as reported previously for many nanocrystalline materials including CeO_2 , Si, Ge, GaAs, and diamond (see References 98, 99, and 100 and references therein).

3. Raman Images

Figure 12.16 illustrates how Raman microspectrometry can be used to image nanophase distribution in nanosized materials. We will present the case of SiC fibers for aerospace applications, prepared with different technologies. These

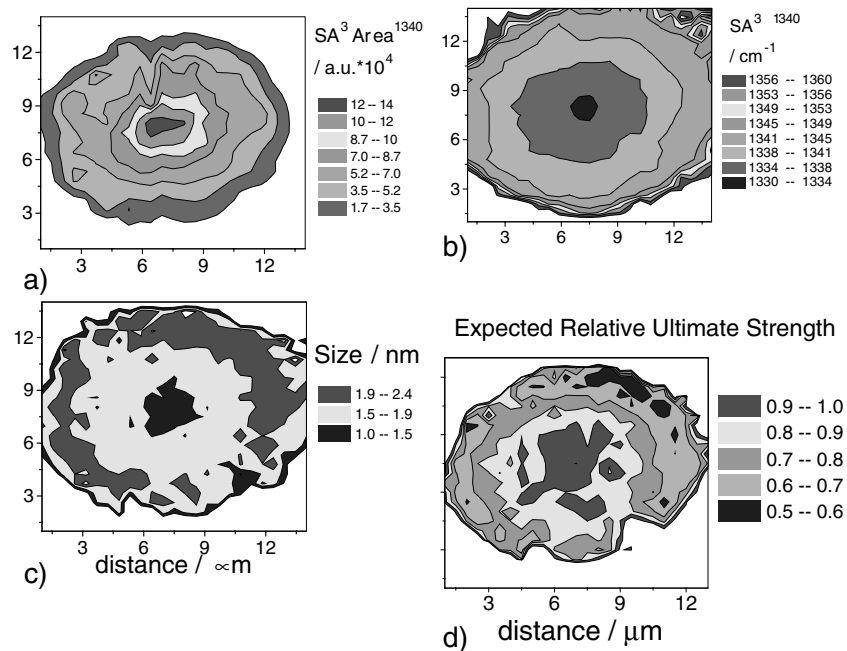
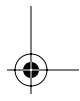
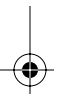
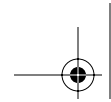


FIGURE 12.16 Raman images of SA3 Ube Industries fiber for D band ($sp^{3/2}$) area (a) and wave number (b) (25×25 spectra, $\lambda = 632$ nm, 0.5 mW, 120 sec/dot). The size distribution of carbon grains was calculated using the correlation between the coherent length and the Raman peaks ratio ID/IG. The relationship correlating Raman studies, TEM examination, and the ultimate strength measurements is used to anticipate the “relative” mechanical strength in the different regions of the fiber (d). (Reprinted from Colombari, P., Raman analysis and “smart” imaging of nanophases and nanosized materials, *Spectroscopy Eur.*, 15, 8, 2003. With permission from Wiley.)





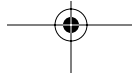
fibers consist of nanosized more or less crystalline SiC grains, with a second phase of disordered carbons. Pure diamond and graphite have sharp peaks at 1331 cm^{-1} and 1581 cm^{-1} , respectively. The two main bands of amorphous carbons are then assigned to diamond-like (D band) and graphite-like (G band) entities. Because the diamond cross section is much lower than that of graphite (approximately 10^2), a weak $\text{C}_{\text{sp}^3}\text{-C}_{\text{sp}^3}$ stretching mode is expected. In fact, given the small size of carbon moieties, the contribution of the chemical bonds located near their surface will be large. The D band can then be assigned to vibrations involving C_{sp^3} -mixed $\text{C}_{\text{sp}^2/\text{sp}^3}$ bonds, hereafter called $\text{sp}^{2/3}$ (assignment of Raman peaks in disordered carbons has been discussed previously^{90,94,97}). This band presents a strong resonant character (contrary to the $\text{sp}^3\text{ C}$ mode in diamond), evidenced by a high dependence of the intensity and position on wavelength.⁹⁰

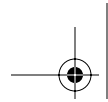
The Tyranno SA3 fiber (UBE Industries Ltd., Ube, Yamaguchi, Japan) is synthesized from graft PCS where methyl groups are replaced by organic groups containing aluminum as a crystal growth inhibitor. Reticulation is obtained by 160°C thermal oxidation, the resulting oxycarbide being carbothermally reduced at 1400°C under inert gas, before decomposition at 1800°C (with CO release). It has been claimed that the glassy silica layer of the SA3 fiber presents a remarkable alkali resistance.¹⁰⁶ The Sylramic fiber (Dow Corning, Midland, MI) is also synthesized from graft PCS, but methyl groups are replaced by organic groups containing boron and titanium. The fiber is made of 96 wt% β -SiC nanocrystals.

The peak area (Figure 12.16a) indicates the concentration of the analyzed phase, the position (wave number, Figure 12.16b) is related to its chemical nature and the wave number comparison gives information on both the nature of the species (especially for resonant lines like the D band at about 1330 cm^{-1}) and the strain level.^{90,94,107} Finally, the bandwidth is related to the phase short-range order. Raman images of SA3 and Sylramic fiber cross sections indicate that core and skin carbon species have a different nature and concentration. The fiber's core is carbon rich and, in the case of the SA3 fiber D band, is up-shifted by $\sim 30\text{ cm}^{-1}$ from the core to the surface. This important shift is due to a transformation of the C-C bond (aromatization). SA3 presents a "carbon-rich tube," while the carbon rate increases gradually from the surface to the core in the Sylramic. This difference between the two fibers can be linked to the elaboration process. During the spinning phase, the viscosity difference between long and short PCS chains leads to concentration gradients. The smallest chains having a lower viscosity could preferentially migrate to the fiber's core. Since they are rich in carbon, due to the high concentration in polymer terminations, they induce carbonated species concentration gradients. These heterogeneities have important consequences on the mechanics of each fiber.

4. Prediction of Material Properties from Raman Parameters

The relationship between grain size and material properties is known for a large number of materials. Once the relationship between Raman parameters and grain size is established, it becomes possible to correlate Raman parameters with the





properties to be achieved in the different parts of the materials. This work was made for CeO_2 , an electrolyte for high-temperature fuel cells and its electrical properties (e.g., the concentration of defects). Raman prediction was in agreement with electrochemical and thermodynamic measurements.^{9,100,101} Prediction of the mechanical properties of SiC fibers from Raman spectra is also possible.

A model has been used to calculate carbon grain size distribution in the as-received SA3 cross section (Figure 12.16c). A ring of larger carbon species appears on the fiber's periphery, indicating a higher short-range order, which is consistent with the decrease in Raman peak widths. This size increase near the surface can be linked to the elaboration process, revealing a higher temperature in this area. Heat-treated fibers show a large increase in this ring. The observed size distribution indicates that crystal growth of the carbon moieties is obtained even deep in the fiber (a small area of low short-range order remains at the core). The relationship between Raman parameters and mechanical properties allows conversion of the Raman image in a predictive "mechanical" image. As an example, we present in Figure 12.16c the expected ultimate strength to be achieved for the different fiber regions. In this example, the highest values are expected from the fiber core. Other types of fibers exhibit homogeneous behavior or an inverse configuration. Note that if a map gives a didactic view, a line scan offers a better compromise between rapidity and quality of information. An example is shown in Figure 12.17 with a line scan ($\sim 18 \mu\text{m}$) between two adjacent NLM SiC fibers in a mullite matrix composite (a ZrO_2 -based coating has been applied onto the fibers).

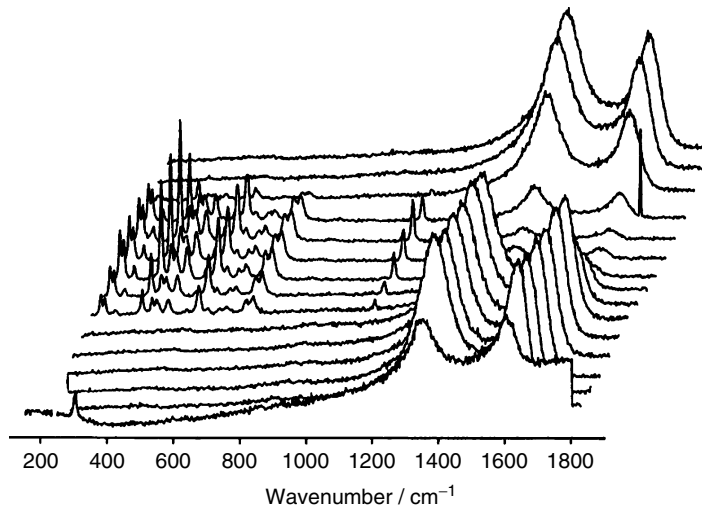
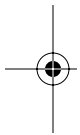
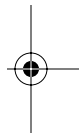
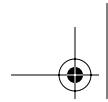


FIGURE 12.17 Spectral in-line scan ($2 \mu\text{m}$ step) of a composite cross section. Spectra were recorded from one NLM202 fiber to another, through the {aluminosilicate + (ZrO_2 ; GeO_2)} tailored interface and the mullite matrix. (Reprinted from Colomban, P., Raman microspectrometry and imaging of ceramic fibers in CMCs and MMCs, 103, 517, 2000. With permission from The American Ceramic Society.)





5. Residual Stress/Strain in Multiphase Materials

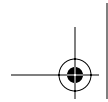
Fiber stress determination is of major importance for the modeling of composites and it is now well established that Raman microspectroscopy, with its main advantage being its nondestructive nature, makes it possible in composites.¹⁰⁷ First, Galiotis¹⁰⁸ and Young¹⁰⁹ demonstrated that Raman spectroscopy is an excellent method to follow the deformation of aramid and carbon fibers. This is a result of variation in the (stretching) vibrational wave number, as a consequence of the anharmonicity of the interatomic bonds. The relationship linking Raman wave number shifts ($\Delta\nu$) to the tensile strain ($\Delta\varepsilon$) is linear, $\Delta\nu = J\Delta\varepsilon$.

It makes it possible to characterize fibers, composites,¹⁰⁷⁻¹¹¹ and films.^{112,113} The only requirement for such studies is to use matrices sufficiently translucent to allow *in situ* recording of the fiber signals through the matrix (a few microns to a few tens of microns inside) and the spectrum of the matrix should not overlap with that of the fibers. The quantitative information on the fiber strain distribution comes from a calibration of the “wave number shift” of the peak against strain. During the last few years, micro-Raman spectroscopy has been increasingly used as a powerful technique to measure local residual stress in submicronic electronic devices. Such localized stresses can induce various types of structural defects modifying the electronic properties. As pointed out in Section III.A, knowledge of the stress concentrations in fiber-reinforced composites is of major importance. Since such stress concentrations cannot be measured easily, many analytical theories have been proposed to understand the micromechanics of composites using the microindentation push-in and push-out tests. Knowledge of Young’s modulus (E), found in the literature or obtained from local microindentation measurements (see Section III.A) allows calculation of the corresponding stress distribution. A shift toward higher energies indicates a compressive strain, whereas a tensile strain corresponds to a decrease in energy. Kevlar fibers display an exceptional strength/stiffness in tension and modulus softening, followed by abrupt “yielding” in compression. On the contrary, in tightly bonded inorganic materials (e.g., SiC), the $|\Delta\nu| = J \times |\Delta\varepsilon|$ relationship is symmetrical. Absolute J values decrease with increasing Young’s modulus.^{107,114} This can be related to the decrease in bond anharmonicity. In the case of an anharmonic potential, the wave number shift increases when high-order transitions are studied. Consequently high-order Raman bands may be preferred for the measurement of stress-induced shifts. Fortunately carbon bonds are present in many fibers and their absorption in the UV-visible range gives rise to a (pre)resonance Raman phenomenon, enhancing the second-order or even the third-order spectra.

VI. SUMMARY

The examples reported in this chapter show that the new processing routes using liquid organometallic ceramic precursors allow the tailoring of multiphase and composite materials at the micro- and nanoscale, and hence the development of functionally graded materials. The stringent advantages are a better control of





the matrix shrinkage during densification, the flexibility of the matrix composition from some mixtures of precursors, and a reduction in the cost and processing time in comparison with the CVI technology.

Depth-sensing microindentation allows the reliable determination of Young's modulus and Vickers' microhardness of the different phases made of grains larger than ~ 2 to $5 \mu\text{m}$. Variations in chemical bonding and short-range order can be extracted from the intensity, wave number, and bandwidth of Raman peaks. The wave number shifts can be used to map the strain (and calculate the stress). Analysis of the bandwidth offers a tool to ascertain whether the wave number shift is strain induced or related to structural evolution of the Raman probe.

Raman spectroscopy provides a better understanding of the material evolution during the materials preparation and aging in operating atmospheres.

ACKNOWLEDGMENTS

The author wishes to thank G. Gouadec, I. Kosacki, M. Parlier, E. Mouchon, E. Bruneton, S. Karlin, V. Vendange, M. Wey, J.L. Lagrange, and C. Courtemanche for their contributions.

REFERENCES

1. Colomban, P., Gel technology in ceramics, glass-ceramics and ceramic-ceramic composites, *Ceram. Int.*, 15, 23, 1989.
2. Colomban, P., Chemical routes and sol-gel processes: the elaboration of ultrafine powders, *Ind. Ceram.*, 792, 186, 1985.
3. Pérez-Arantegui, J., Molera, J., Larrea, A., Pradell, T., Vendrell-Saz, M., Borgia, I., Brunetti, B.G., Cariati, F., Fermo, P., Mellini, M., Sgamellotti, A., Viti, C., Luster pottery from the thirteenth century to the sixteenth century: a nanostructured thin metallic film, *J. Am. Ceram. Soc.*, 84, 442, 2001.
4. Karlin, S., Colomban, P., Phase diagram, short range structure and amorphous phases in the $\text{ZrO}_2\text{-GeO}_2\text{-H}_2\text{O}$ system, *J. Am. Ceram. Soc.*, 82, 735, 1999.
5. Segal, D., *Chemical Synthesis of Advanced Ceramic Materials*, Cambridge University Press, Cambridge, 1989.
6. Perthuis, H., and Colomban, P., Well densified NASICON-type ceramics elaborated using sol-gel process and sintering at low temperatures, *Mater. Res. Bull.*, 19, 621, 1984.
7. Perthuis, H., and Colomban, P., Sol-gel routes leading to NASICON ceramics, *Ceram. Int.*, 12, 39, 1986.
8. Mazdiyasi, K.S., Powder synthesis from metal-organic precursors, *Ceram. Int.*, 8, 42, 1982.
9. Yoldas, B.E., Effect of variation in polymerized oxides on sintering and crystalline transformations, *J. Am. Ceram. Soc.*, 65, 387, 1977.
10. Sakka, S., and Kamiya, K., Glasses from metal alcoholates, *J. Non-Crystl. Solids*, 42, 403, 1980.
11. Johnson, D.W., Jr., Sol-gel processing of ceramics and glass, *Am. Ceram. Soc. Bull.*, 64, 1587, 1985.





12. Colomban, P., and Wey, M., Sol-gel control of the matrix net-shape sintering in 3D reinforced ceramic matrix composites, *J. Eur. Ceram. Soc.*, 17, 1475, 1997.
13. Okamura, H., and Bowen, H.K., Preparation of alkoxides for the synthesis of ceramics, *Ceram. Int.*, 12, 161, 1986.
14. Bruneton, E., Bigarré, J., Michel, D., and Colomban, P., Heterogeneity, nucleation, shrinkage and bloating in sol-gel glass ceramics: the case of LAS compositions, *J. Mater. Sci.*, 32, 3541, 1997.
15. Klein, L.C., Ed., *Sol-Gel Technology*, Noyes Publications, Park Ridge, NJ, 1988.
16. Colomban, P., Raman studies of inorganic gels and of their sol-to-gel, gel-to-glass and glass-to-ceramic transformation, *J. Raman Spectrosc.*, 27, 747, 1996.
17. Pouxviel, J.C., Boilot, J.P., Dauger, A., and Wright, A., Gelation study of aluminosilicates by small-angle neutron scattering, *J. Non-Crystl. Solids*, 103, 331, 1988.
18. Pouxviel, J.C., Boilot, J.P., Smaïhi, M., and Dauger, A., Structural study of aluminosilicate sols and gels by SAXS and SANS, *J. Non-Crystl. Solids*, 106, 147, 1988.
19. Poorteman, M., Descamps, P., Cambier, F., Plisnier, M., Canonne, V., and Descamps, J.C., Silicon nitride/silicon carbide nanocomposite obtained by nitridation of SiC: fabrication and high temperature mechanical properties, *J. Eur. Ceram. Soc.*, 23, 2361, 2003.
20. Yajima, S., Okamura, K., Hayashi, J., and Omori, M., Development of a SiC fibre with high tensile strength, *Nature*, 261, 683, 1976.
21. Yajima, S., Okamura, K., Hayashi, J., and Omori, M., Synthesis of continuous SiC fibre with a high tensile strength, *J. Am. Ceram. Soc.*, 59, 324, 1976.
22. Noireaux, P., Jamet, J., Parlier, M., and Bacos, M.P., Polysilanes et leur procédé de préparation, French Patent no. FR 2642080, July 27, 1990.
23. Parlier, M., and Colomban, P., Composites à matrice céramique pour applications thermosturales, *Recherche Aérospatiale*, 5–6, 457, 1996.
24. Colomban, P., and Vendange, V., Sintering of alumina and mullite prepared by slow hydrolysis of alkoxides: the role of the protonic species and of pore topology, *J. Non-Crystl. Solids*, 147, 245, 1992.
25. Bruneton, E., and Colomban, P., Influence of hydrolysis conditions on crystallization, phase transitions and sintering of zirconias prepared by alkoxide hydrolysis, *J. Non-Crystl. Solids*, 147, 201, 1992.
26. Vendange, V., and Colomban, P., Densification mechanisms of alumina, aluminosilicates and aluminoborosilicates gels, glasses and ceramics, *J. Sol-Gel Sci. Technol.*, 2, 407, 1994.
27. Colomban, P., Protonic defects and crystallization of Sol-Gel (Si,Ge) mullites and alumina, *Ceramics Today — Tomorrow's Ceramics*, P. Vincenzini, Ed., *Mater. Sci. Monogr.*, 66B, 599, 1991.
28. Colomban, P., Courret, H., Romain, F., Gouadec, G., and Michel, D., Sol-gel prepared pure and Li-doped hexacelsian polymorphs. An infrared, Raman and thermal expansion study of β -phase stabilization by frozen short-range disorder, *J. Am. Ceram. Soc.*, 83, 2974, 2000.
29. Roy, R., Gel route to homogeneous glass preparation, *J. Am. Ceram. Soc.*, 52, 344, 1969.
30. Vendange, V., and Colomban, P., How to tailor the porous structure of alumina and aluminosilicate gels and glasses, *J. Mater. Res.*, 11, 518, 1996.





31. Vendange, V., and Colombar, P., Determination of the hydroxyl group content in gels and porous "glasses" issued of alkoxide hydrolysis by combined TGA and BET analysis, *J. Porous Mater.*, 3, 193, 1996.
32. Roy, D.M., and Roy, R., Synthesis and stability of minerals in the system $MgO-Al_2O_3-SiO_2-H_2O$, *Am. Miner.*, 40, 147, 1955.
33. Vendange, V., Colombar, P., and Larché, F., Pore size and liquid impregnation of microporous aluminosilicate gels and glasses, *Microporous Mater.*, 5, 389, 1996.
34. Howe, A.T., and Shilton, M., Densification of HUP solid electrolyte, *J. Solid State Chem.*, 34, 341, 1980.
35. Colombar, P., Ed., *Proton Conductors—Solids, Membranes and Gels—Materials and Devices*, Cambridge University Press, Cambridge, 1992.
36. Bouquin, O., Perthuis, H., and Colombar, P., Low temperature sintering and optimal physical properties: a challenge the NASICON ceramics case. *J. Mater. Sci. Lett.*, 4, 956, 1985.
37. Lagrange, J.L., and Colombar, P., Double particle reinforcement of ceramic matrix composites prepared through a sol-gel route, *Composites Sci. Technol.*, 58, 653, 1998.
38. Rigacci, A., Achard, P., Ehrburger-Dolle, F., and Pirard, R., Structural investigation in monolithic silica aerogels and thermal properties, *J. Non-Crystl. Solids*, 225, 260, 1998.
39. di Costanzo, T., Frappart, C., Mazerolles, L., Rouchaud, J.C., Fedoroff, M., Michel, D., Beauvy, M., Vignes, J.L., Fixation de divers polluants dans des alumines monolithiques poreuses, *Ann. Chim. Sci. Mater.*, 26, 67, 2001.
40. Sherer, G.W., Calas, S., and Sempéré, R., Densification kinetics and structural evolution during sintering of silica aerogel, *J. Non-Crystl. Solids*, 240, 118, 1998.
41. Colombar, P., Frittage de céramiques transparentes PLZT, *Ind. Ceram.*, 697, 531, 1976.
42. Lenfant, P., Plas, D., Ruffo, M., Boilot, J.-P., and Colombar, P., Céramiques d'alumine et de ferrite pour sonde à protons, *Mater. Res. Bull.*, 15, 1817, 1980.
43. Perthuis, H., and Colombar, P., Li^+ eucryptite superionic thick films, *J. Mater. Sci. Lett.*, 4, 344, 1985.
44. Perthuis, H., Velasco, G., and Colombar, P., Na^+ and Li^+ NASICON superionic conductor thick films, *Jpn. J. Appl. Phys.*, 23, 534, 1984.
45. Colombar, P., Boilot, J.-P., Polymères inorganiques (xerogels et verres) dans les systèmes $M_2O-M'O_2SiO_2-P_2O_5X_2O_3$, *Rev. Chim. Miner.*, 22, 235, 1985.
46. Blanchard, N., Boilot, J.-P., Colombar, P., Pouxviel, J.-C., New glasses from metal-organic precursors: preparation and properties, *J. Non-Crystl. Solids*, 82, 205, 1986.
47. Colombar, P., Sol-gel synthesis and densification of NASICON powders, *Adv. Ceram.*, 21, 139, 1987.
48. Boilot, J.P., Gay, A., Colombar, P., Lejeune, M., Compositions solides amorphes et homogènes à base de dérivés métalliques, sous forme de gels polymérisés ou de verres, leur préparation et leur application, French Patent (CNRS) no. EN 83 06 934.
49. Colombar, P., and Mazerolles, L., Nanocomposites in mullite- ZrO_2 and mullite- TiO_2 systems synthesized through alkoxide hydrolysis gel routes. Microstructure and fractography, *J. Mater. Sci.*, 26, 3503, 1991.



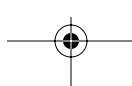
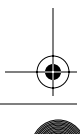
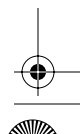


50. Colomban, P., and Mazerolles, L., SiO₂-Al₂O₃ phase diagram and mullite non-stoichiometry of sol-gel prepared monoliths: influence on mechanical properties, *J. Mater. Sci. Lett.*, 2, 1077, 1990.
51. Colomban, P., Structure of oxide gels and glasses by IR and Raman scattering: I. Aluminas, *J. Mater. Sci.*, 24, 3002, 1989.
52. Colomban, P., Structure of oxide gels and glasses by IR and Raman scattering: II. Mullites, *J. Mater. Sci.*, 24, 3011, 1989.
53. Snow, G., Fabrication of transparent electronic PLZT ceramics by atmosphere sintering, *J. Am. Ceram. Soc.*, 56, 91, 1973.
54. Haertling, G.H., Ferroelectric ceramics: history and technology, *J. Am. Ceram. Soc.*, 82, 797, 1999.
55. Erikson, D.D., Wood, T.E., and Wood, W.P., Historical development of abrasive grain, Sol-gel processing symposium, *Ceram. Trans.*, 12, 95, 1998.
56. Sowman, H.G., U.S. Patent nos. 3,795,524, 3,709,706, 3,793,041, 3,916,584, 4,047,965, 4,125,406.
57. Whitney, E.D., and Vaidyanathan, P.N., Microstructural engineering of ceramic cutting tools, *Am. Ceram. Soc. Bull.*, 67, 1010, 1988.
58. Mathers, J.P., Forester, T.E., and Wood, W.P., Sol-gel preparation of non-oxide abrasives, *Am. Ceram. Soc. Bull.*, 68, 130, 1989.
59. Hamasaki, T., Eguchi, K., Koyanagi, K., Matsumoto, A., Utsunomiya, T., and Koba, K., Preparation and characterization of machinable mica/glass-ceramics by sol-gel process, *J. Am. Ceram. Soc.*, 71, 1120, 1988.
60. Hoffman, D., Roy, R., and Komarneni, S., Diphasic ceramic composites via a sol-gel method, *Mater. Lett.*, 2, 245, 1984.
61. Roy, R.A., and Roy, R., Diphasic xerogels: I. Ceramics metal composites, *Mater. Res. Bull.*, 19, 169, 1984.
62. Petrullat, J., Ray, S., Schubert, U., Guldner, G., Egger, C., and Breitscheidel, B., Preparation and processing of metal-ceramic composite materials, *J. Non-Cryst. Solids*, 147, 594, 1992.
63. Breval, E., Deng, Z., Chiou, S., and Pantano, C.G., Sol-gel prepared Ni-alumina composite materials. Part I, Microstructure and mechanical properties. *J. Mater. Sci.*, 27, 1464, 1992.
64. Stella, A., Cheyssac, P., De Silvestri, S., Kofman, R., Lanzani, G., Nisoli, M., Tognini, P., Self organized growth and ultrafast electrodynamic dynamics in metallic nanoparticles, in *Nanophase and Nanocomposite Materials II*, S. Komarneni, J.C. Parker, and H.J. Wollenberger, Eds., *Mater. Res. Soc. Symp. Proc.*, 457, 155, 1997.
65. Vendange, V., and Colomban, P., Elaboration and thermal stability of alumina, alumino-silicate. Fe, Co, Ni magnetic nanocomposites prepared through a sol-gel route, *Mater. Sci. Eng. A*, 168, 199, 1993.
66. Colomban, P., and Vendange, V., Sol-gel routes towards magnetic nanocomposites with tailored microwave absorption, in *Nanophase and Nanocomposite Materials II*, S. Komarneni, J.C. Parker, and H.J. Wollenberger, eds., *Mater. Res. Soc. Symp. Proc.*, 457, 451, 1997.
67. Mouchon, E., and Colomban, P., Microwave absorbent: preparation, mechanical properties and RF/microwave conductivity of SiC (and/or mullite) fibres reinforced NASICON matrix composites, *J. Mater. Sci.*, 31, 323, 1996.
68. Naslain, R., Fiber-matrix interphases and interfaces in ceramic matrix composites processed by CVI, *Composite Interfaces*, 1, 253, 1993.



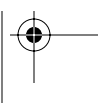


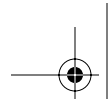
69. Droillard, B., Lamon, J., and Bourrat, X., Strong interfaces in CMCs-conditions for efficient multilayered interphases, *Mater. Res. Soc. Symp. Proc.*, 365, 371, 1995.
70. Qui, D., and Pantano, C.G., Sol-gel processing of carbon fiber-reinforced glass matrix, in *Ultrastructure Processing of Ceramics, Glasses and Composites*, J.D. Mackenzie and D.R. Ulrich, Eds., John Wiley & Sons, New York, 1987.
71. Panhorst, W., Spallek, M., Brueckner, R., Hegaler, H., Reich, C., Gratewohl, G., Meier, B., Spelmann, D.S., Fibre-reinforced glass ceramics fabricated by a novel process, *Ceram. Eng. Sci. Proc.*, 11, 947-63, 1990.
72. Russell-Floyd, R.S., Harris, B., Cooke, R.G., Laurie, J., Hammett, F.W., Jones, R.W., Wang, T., Application of sol-gel processing techniques for the manufacture of fiber-reinforced ceramics, *J. Am. Ceram. Soc.*, 76, 2635, 1993.
73. Guney, V., Jones, F.R., James, P.F., and Bailey, J.E., Alumina ceramic matrices for fibre composites prepared by modified sol-gel processing, Institute of Physics Publishing, London, 1990.
74. Wu, J., Chen, M., Jones, F.R., and James, P.F., Mullite matrix fibre reinforced composites by sol-gel processing, *Ceram. Trans.*, 46, 177, 1995.
75. Wu, J., Chen, M., Jones, F.R., and James, P.F., Characterization of sol-gel derived alumina-silica matrices for continuous fibre reinforced composites, *J. Eur. Ceram. Soc.*, 16, 619, 1996.
76. Colomban, P., Process for fabricating a ceramic matrix composite incorporating woven fibers and materials with different compositions and properties in the same composite, *Mater. Technol.*, 10, 89, 1995.
77. Colomban, P., Menet, M., Mouchon, E., Courtemanche, C., and Parlier, M., Composites céramique-céramique multicouches élaborés en utilisant un précurseur d'interface et un précurseur de matrice [Multilayer fiber-matrix ceramic composite material and process for its production], French Patent nos. (ONERA) FR 2672283 (Feb. 4, 1991) and EP 0 498 698 (Jan. 29, 1992), and U.S. Patent no. 07/830.904.
78. Colomban, P., Bruneton, E., Lagrange, J.L., Mouchon, E., Sol-gel mullite matrix-SiC and -mullite 2D woven fabrics composites with or without zirconia containing interphase. Elaboration and properties, *J. Eur. Ceram. Soc.*, 16, 301, 1996.
79. Colomban, P., and Lapous, N., New sol-gel matrices of chemically stable composites BAS, NAS and CAS, *Composites Sci. Technol.*, 56, 737, 1996.
80. Mouchon, E., and Colomban, P., Oxide ceramic matrix-oxide fibers woven fabric composites exhibiting dissipative fracture behavior, *Composites*, 26, 175, 1995.
81. Colomban, P., Composites céramiques multiniredux ou l'intérêt des méthodes sol-gel, Proc. 8^e Journées Nationales sur les composites, JNC'8, Alix, O., Favre, J.P., and Ladevèze, P., Eds., AMAC, Paris, 1992, 73.
82. Jamet, J., Demange, D., and Loubeau, J., Procédé d'élaboration de composites, French Patent no. (ONERA) FR 2526785 (Nov. 18, 1985).
83. Colomban, P., Wey, M., and Parlier, M., Procédé d'élaboration d'un matériau céramique par infiltration d'un précurseur dans un support poreux céramique, French Patents (ONERA) FR 2713222 (June 9, 1995), EP 0.656.329 (Jan. 31, 1995), and 0656329 (June 17, 1998).
84. Touati, F., Gharbi, N., and Colomban, P., Structural evolution in polyolysed hybrid organic-inorganic alumina gels, *J. Mater. Sci.*, 35, 1565, 2000.
85. Parlier, M., and Ritti, M.H., State of the art and perspective for oxide-oxide composites, *Aerospace Sci. Technol.*, 7, 211, 2003.



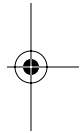


86. Colomban, P., Sol-gel route to functional and hierarchical ceramic matrix composites, in Proceedings ICIM '96, ECSSM '96, Lyon '96, 3rd International Conference on Intelligent Materials, June 3–5, 1996, P.F. Gobin and J. Tatibouet, Eds., SPIE, Lyon, 1996.
87. Colomban, P., Sol-gel control of the micro/nanostructure of functional ceramic-ceramic and metal-ceramic composites, *J. Mater. Res.*, 13, 803, 1998.
88. Loubet, J.L., Georges, J.M., Marchesini, O., and Meille, G., Vickers indentation curves of magnesium oxide, *J. Tribol.*, 106, 43, 1984.
89. Colomban, P., Tailoring and control of the micro/nanostructure of functional (FGM) CMC's and MMC's, *J. Korean Ceram. Soc.*, 5, 55, 1999.
90. Gouadec, G., Colomban, P., and Bansal, N.P., Raman study of Hi-nicalon fiber reinforced celsian composites. Part I: Distribution and nanostructure of different phases, *J. Am. Ceram. Soc.*, 84, 1129, 2001.
91. Gouadec, G., Colomban, P., and Bansal, N.P., Raman study of Hi-nicalon fiber reinforced celsian composites. Part II: Residual stress in the fibers, *J. Am. Ceram. Soc.*, 84, 1136, 2001.
92. Hsueh, C.H., Interfacial debonding and pull-out stresses of fiber reinforced composites, *Mater. Sci. Eng. A*, A154, 125, 1992.
93. Marshall, D.B., Analysis of fiber debonding and sliding experiments in brittle matrix composites, *Acta Metal. Mater.*, 40, 427, 1992.
94. Colomban, P., Stress- and nanostructure-imaging of ceramic fibers and abradable thermal barrier coatings by Raman microspectrometry—state of the art and perspectives, Proceedings of the 24th Annual Cocoa Beach Conference and Exposition, Cocoa Beach, Florida, Jan. 23–28, 2000, T. Jessen and E. Ustundag, Eds., *Ceram. Eng. Sci. Proc.*, 21, 143, 2000.
95. Colomban, P., and Havel, M., Raman imaging of stress-induced phase transformation in transparent ZnSe ceramics and sapphire single crystal, *J. Raman Spectrosc.*, 33, 789, 2002.
96. Havel, M., and Colomban, P., Rayleigh and Raman image of the bulk/surface surface nanostructure of SiC based fibres, *Composite B Eng.*, 35B, 353, 2004.
97. Havel, M., and Colomban, P., Skin/bulk nanostructure and corrosion of SiC based fibres. A surface Rayleigh and Raman study, *J. Raman Spectrosc.*, 34, 786, 2003.
98. Colomban, P., Raman/Rayleigh study of nanophases, Proceedings of the 27th Annual Cocoa Beach Conference and Exposition, Cocoa Beach, Florida, January 26–31, 2003, W.H. Kriven and H.T. Lin, Eds., *Ceram. Eng. Sci. Proc.*, 24, 41, 2003.
99. Gouadec, G., and Colomban, P., Raman spectroscopy of nanomaterials: how do spectra relate to particle size and local mechanics?, Progress in crystal growth, in press, 2005.
100. Suzuki, T., Kosacki, I., Colomban, P., and Anderson, H.U., Electrical conductivity and lattice defects in nanocrystalline CeO₂ thin films, *J. Am. Ceram. Soc.*, 84, 2007, 2001.
101. Kosacki, I., Suzuki, T., Anderson, H., and Colomban, P., Raman scattering and lattice defects in nanocrystalline CeO₂ thin films, *Solid State Ionics*, 149, 99, 2002.
102. Surca-Vuk, A., Orel, B., Drazic, G., and Colomban, P., Vibrational spectroscopy and analytical electron microscopy studies of Fe-V-O and In-V-O thin films, in *Nanostructured Materials*, H. Hofman, Z. Rahman, U. Schubert, Eds., Springer, Wien, 2002.





103. Parayanthal, P., and Pollak, F.H., Raman scattering in alloy semiconductors: "spatial correlation" model, *Phys. Rev. Lett.*, 52, 1822, 1984.
104. Solin, S.A., and Caswell, N., Raman scattering from alkali graphite intercalation compounds, *J. Raman Spectrosc.*, 10, 129, 1981.
105. Duval, E., Far-infrared and Raman vibrational transitions of a solid sphere: selection rules, *Phys. Rev. B*, 46, 5795, 1992.
106. Ishikawa, T., Kohtoku, Y., Kumagawa, K., Yamamura, T., and Nagasawa, T., High-strength alkali-resistant sintered SiC fibre stable to 2200°C, *Nature*, 391, 773, 1998.
107. Colomban, P., Analysis of strain and stress in ceramic, polymer and metal matrix composites by Raman spectroscopy, *Adv. Eng. Mater.*, 4, 535, 2002.
108. Galiotis, C., Laser Raman spectroscopy, a new stress/strain measurement technique for the remote and on-line non-destructive inspection of fiber reinforced polymer composites, *Mater. Technol.*, 8, 203, 1993.
109. Young, R.J., Raman spectroscopy and mechanical properties, in *Characterization of Solid Polymers*, S.J. Spelles, Ed., Chapman & Hall, London, 1994.
110. Beyerlein, J., Amer, M.S., Schadler, L.S., and Phoenix, S.L., New methodology for determining *in situ* fiber, matrix and interface stresses in damaged multifiber composites, *Sci. Eng. Composite Mater.*, 7, 151, 1998.
111. Wu, J., and Colomban, P., Raman spectroscopy study on the stress distribution in the continuous fibre reinforced ceramic matrix composites, *J. Raman Spectrosc.*, 28, 523, 1997.
112. Mohrbacker, H., Van Acker, K., Blanpain, B., Van Houtte, P., and Celis, J.P., Comparative measurement of residual stress in diamond coatings by low-incident-beam-angle-diffraction and micro-Raman spectroscopy, *J. Mater. Res.*, 11, 1776, 1996.
113. de Wolf, I., Vanhellefont, J., Romano-Rodriguez, A., Norström, H., and Maes, H.E., Micro-Raman study of stress distribution in local isolation structure and correlation with transmission electron spectroscopy, *J. Appl. Phys.*, 71, 898, 1992.
114. Gouadec, G., and Colomban, P., Non-destructive mechanical characterization of SiC fibers by Raman spectroscopy, *J. Eur. Ceram. Soc.*, 21, 1249, 2001.



Chemical Processing of Ceramics

Second Edition

edited by
Burtrand Lee
Sridhar Komarneni



Taylor & Francis
Taylor & Francis Group

Boca Raton London New York Singapore

A CRC title, part of the Taylor & Francis imprint, a member of the
Taylor & Francis Group, the academic division of T&F Informa plc.



Published in 2005 by
CRC Press
Taylor & Francis Group
6000 Broken Sound Parkway NW, Suite 300
Boca Raton, FL 33487-2742

© 2005 by Taylor & Francis Group, LLC
CRC Press is an imprint of Taylor & Francis Group

No claim to original U.S. Government works
Printed in the United States of America on acid-free paper
10 9 8 7 6 5 4 3 2 1

International Standard Book Number-10: 1-57444-648-7 (Hardcover)
International Standard Book Number-13: 978-1-57444-648-7 (Hardcover)
Library of Congress Card Number 2004065504

This book contains information obtained from authentic and highly regarded sources. Reprinted material is quoted with permission, and sources are indicated. A wide variety of references are listed. Reasonable efforts have been made to publish reliable data and information, but the author and the publisher cannot assume responsibility for the validity of all materials or for the consequences of their use.

No part of this book may be reprinted, reproduced, transmitted, or utilized in any form by any electronic, mechanical, or other means, now known or hereafter invented, including photocopying, microfilming, and recording, or in any information storage or retrieval system, without written permission from the publishers.

For permission to photocopy or use material electronically from this work, please access www.copyright.com (<http://www.copyright.com/>) or contact the Copyright Clearance Center, Inc. (CCC) 222 Rosewood Drive, Danvers, MA 01923, 978-750-8400. CCC is a not-for-profit organization that provides licenses and registration for a variety of users. For organizations that have been granted a photocopy license by the CCC, a separate system of payment has been arranged.

Trademark Notice: Product or corporate names may be trademarks or registered trademarks, and are used only for identification and explanation without intent to infringe.

Library of Congress Cataloging-in-Publication Data

Chemical processing of ceramics.—2nd ed. / edited by Burtrand Lee and Sridhar Komarneni.
p. cm.— (Materials engineering ; 28)
Includes bibliographical references and index.
ISBN 1-57444-648-7 (alk. paper)
1. Ceramics—Analysis. 2. Ceramic materials. I. Lee, Burtrand Insung. II. Komarneni, Sridhar. III. Title. IV. Series: Materials engineering (Marcel Dekker, Inc.) ; 28.

TP810.5.C48 2005
666—dc22

2004065504



Taylor & Francis Group
is the Academic Division of T&F Informa plc.

Visit the Taylor & Francis Web site at
<http://www.taylorandfrancis.com>

and the CRC Press Web site at
<http://www.crcpress.com>

